Breaking Characteristics and Geometric Properties of Spilling Breakers over Slopes

Mayilvahanan Alagan Chella[1]*, Hans Bihs[1], Dag Myrhaug[2], Michael Muskulus[1]

[1]Department of Civil and Environmental Engineering

[2]Department of Marine Technology

Norwegian University of Science and Technology (NTNU), 7491 Trondheim, Norway

Abstract

A two-phase flow CFD model based on the Reynolds-Averaged-Navier-Stokes (RANS) equations coupled with the level set method (LSM) and $k - \omega$ turbulence model is used to simulate spilling breakers over a sloping bed. In order to validate the present numerical model, the simulated results are compared with the experimental data measured by Ting and Kirby (1996). The simulated horizontal velocities and free surface elevations are in good agreement with the experimental measurements. Moreover, the present model is able to model the prominent features associated with the breaking process such as the motion of air pockets in the water, formation of a forward moving jet, the splash-up phenomenon and the mixing of air and water in the breaking region. The numerical model has been utilized to study the influences of three important environmental parameters; water depth, offshore wave steepness and beach slope on the characteristics and geometric properties of spilling breakers over slopes. A total of 39 numerical experiment cases are performed to investigate the characteristics of breaking waves such as breaking location, incipient breaker height and water depth at breaking, incipient breaker indices and geometric properties with different offshore wave steepnesses at different water depths over a wide range of beach slopes. The geometric properties associated with breaking waves in shallow water are described using the wave steepness and asymmetry factors introduced by Kjeldsen and Myrhaug (1978). The computed results appear to give reasonable predictions and consistency with previous studies.

Keywords:

Breaking waves, wave profile asymmetry, spilling breakers, numerical modeling, breaker indices

1 Introduction

Wave breaking is a natural process involving transformation of wave energy into turbulent energy leading to a violent transformation of the free surface, that exerts massive hydrodynamic loads on marine structures (Cokelet, 1977). During wave breaking for shoaling waves, the dissipation of energy takes place in order to approximately balance the increase in the local wave energy due to shoaling. However, the wave breaking process is primarily responsible for the creation of the surface turbulence and is increasing the turbulent kinetic energy, that plays an important role in the vertical mixing of momentum through the water column (Craig, 1996; Ting and Kirby, 1996). Massel (2007)gives a wide perspective of the breaking of both regular and random waves and how this is linked with the aerosol production and air-sea gas interaction. Based on the steepness of the wave and the seabed slope, breaker types can be categorized into four different types, namely spilling, plunging, surging and collapsing (Galvin, 1968). The breaking process depends on many physical parameters; water depth, wave height, wave length and sea bed slope. Breaking waves are three-dimensional (3D) due to the interaction with waves, current or wind in a real sea environment. Moreover, e.g. in a wave tank waves always begin to propagate down the tank as undisturbed two-dimensional (2D) waves and reach the critical point at which the unstable water front evolves into a 3D flow. Therefore, 2D models can capture most of the wave breaking characteristics up to the breaking point, where 3D effects are minimal. A symmetrical wave can be expressed by the wave steepness. As

$$\varepsilon = \frac{\eta'}{L'} \qquad \delta = \frac{\eta'}{L''} \qquad \lambda = \frac{L''}{L'} \qquad \mu = \frac{\eta'}{H_b}$$
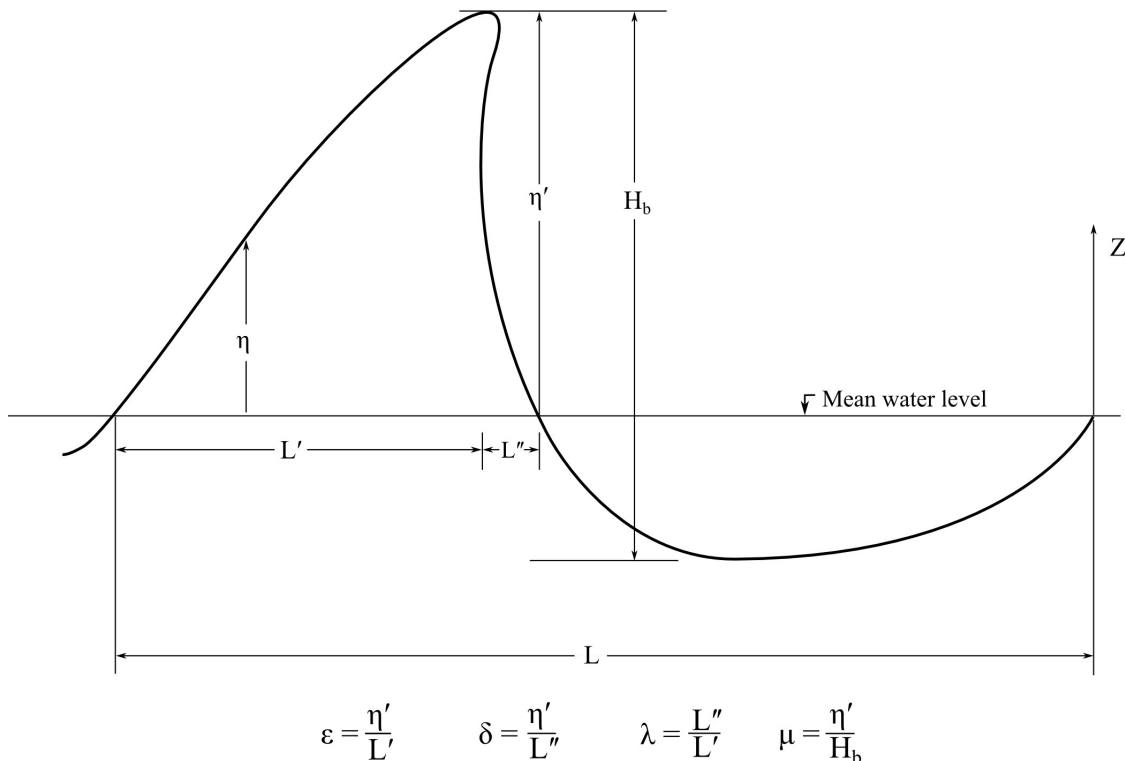
Figure 1: Definition sketch of local wave geometry parameters following Kjeldsen and Myrhaug (1978)

it propagates over a plane slope, the wave starts to deform and the wave front moves forward, thus the shape of the wave profile is not symmetric anymore. Several studies have been carried out to investigate the geometric properties of breaking waves in deep water (Kjeldsen and Myrhaug, 1978; Bonmarin, 1989; Lader, 2002; Babanin et al., 2010). Although a considerable amount of literature has been reported on wave steepness and asymmetry factors of shallow water waves (Ippen and Kulin, 1954; Miller and Zeigler, 1964; Adeyemo, 1968; Iwagaki and Sakai, 1972), there has been limited studies on the geometrical asymmetry associated with breaking waves on slopes in shallow water. A definition sketch of the wave asymmetry profile at breaking in shallow water is shown in Fig. 1. The breaking asymmetry profile parameters can be related to breaking wave forces on coastal structures, which influence the global design of a structure (Adeyemo, 1968). Much uncertainty still exists about the relationship between the wave asymmetry profile parameters and the breaking wave forces, suggesting a need to understand the geometric properties of breaking waves on slopes in shallow water and the effect of breaking wave forces on coastal structures. The maximum wave height governs the critical design condition for coastal structures, which is greatly influenced by the wave breaking process.

The wave transformation over a sloping bed, such as shoaling, overturning and onset of wave breaking can be described theoretically or numerically by classical potential flow theory. However, this disregards the influence of viscosity and turbulence production, which plays a vital role in wave breaking, especially for waves over sloping beds. The first numerical computation of breaking waves in deep water was performed by Longuet-Higgins and Cokelet (1976) by applying a mixed Eulerian-Lagrangian formulation (MEL) with the boundary integral method based on potential theory and a conformal mapping of physical plane limited to a periodic domain in deep water. Vinje and Brevig (1981) applied the same method in the physical plane, and they extended the application to finite water depth. Most recent MEL based models are capable of modeling both arbitrary waves and water depths. The MEL method is able to model the breaking waves until breaking but can not model the interface reconnection phenomenon that occurs during the breaking process (Chen et al., 1999). Other models based on the Boussinesq approximation have been used to simulate only the wave deformation. This method can not be used directly to model the wave breaking (Christensen, 1998), but the model can be used to calculate the wave transformation in the surf zone together with a model for the dissipation of energy. The description of the breaking process is highly demanding due to unsteady non-linear viscous flow, the complex air-water interface, small scale free surface turbulence transport and dissipation process. Moreover, the theoretical description of the entire process is only possible with gross simplifications and assumptions (Cokelet, 1977). Thus, most of the studies on breaking waves are limited to field and laboratory experiments. Many theories and formulas to predict the breaking wave characteristics have been proposed based on the physical experiments (Goda, 2010; Iwagaki and Sakai, 1972; Tsai et al., 2005). Due to the complexity in describing wave breaking process, most of the existing formulas are empirical and semi-empirical, and thus subjected to the experimental conditions and scale effects. However, none of the relationships have been established globally for obtaining the breaking wave properties for practical engineering applications (Southgate, 1993).

An efficient model based on Computational Fluid Dynamics (CFD) can describe the wave breaking process without specifying breaking criteria. The prominent features of the physical process can be obtained in detail without much simplifications, assumptions and approximations in the fluid flow properties (Christensen, 1998). CFD solves the fundamental fluid

dynamic equations including the air-water interface. The small scale free surface turbulence transport and dissipation process can be represented by a suitable turbulence model. Hence, the method is capable of determining the detailed information concerning fluid flow properties such as velocities, turbulence, interface deformation etc. A number of numerical studies based on viscous computations attempted to simulate the breaking process with a single phase model such as Lin and Liu (1998), Bradford (2000) and Zhao et al. (2004). Since a single phase model ignores the motion of the air over the free surface and the density variation across the interface, which are primarily responsible for the surface deformation phenomenon, the complete description of the breaking process is still not fully represented. Hence, all the previously mentioned models have some significant discrepancies compared with the experimental data. Other studies such as Chen et al. (1999), Hieu et al. (2004), Christensen (2006), Jacobsen et al. (2012) used a two-phase flow model to describe the wave breaking process. Detailed literature reviews on the methods and results can be found in Lin and Liu (1998), Chen et al. (1999), Zhao et al. (2004), Hieu et al. (2004) and Bradford (2000). Christensen (2006) studied the undertow profiles and turbulence levels in breaking waves with a Navier-Stokes solver and the volume of fluid method (VOF). The Large Eddy Simulation (LES) technique is used to model the turbulence in the breaking waves. The predicted turbulence levels and the wave heights at breaking were higher than in the experiments. Jacobsen et al. (2012) presented the application of OpenFOAM to model spilling breaking waves using the Reynolds-Averaged Navier-Stokes equations (RANS) equations, coupled with the VOF method. They compared the numerical results with the experimental data by Ting and Kirby (1996) using a geometric cut-off (i.e. a significant modification at the end of the tank). Moreover, their model slightly over-predicted the wave crest height before the breaking point and under-predicted the wave crest height in the surf zone. These studies proposed to model the undertow profiles, turbulence levels and turbulent characteristics for different types of breakers. However, uncertainty still exists about the relationship between the environmental parameters, characteristics and geometrical properties of wave breaking on slopes.

The purpose of the present work is to investigate the effects of water depth, offshore wave steepness, and beach slope on the characteristics and geometric properties of spilling breakers over slopes. A 3D two-phase flow CFD model solving the RANS equations is applied in a 2D setting to simulate the breaking waves with the level set method to capture the air-water interface deformation. Although wave breaking is a 3D process, most of the physical characteristics inducing wave breaking can be obtained in detail by a 2D study. To validate the present numerical model, the results from the simulation of breaking waves over a sloping bed are compared with the experimental data by Ting and Kirby (1996). The simulated results are in good agreement with experimental measurements. The characteristics of breaking waves such as breaking location, the incipient breaker height and water depth at breaking, incipient breaker indices and geometric properties for different offshore wave steepnesses at different water depths over a wide range of beach slopes are also examined and discussed.

1.1   Wave breaking

When waves propagate from deep to shallow water, the wave motion is restricted by the change in water depth; e.g the wave celerity is reduced. Since the wave period remains the same, the wave length becomes shorter, resulting in increased wave heights. The behaviour of long waves over a sloping bed is strongly affected by the wave base, which is the depth at which the wave

motion becomes negligible, i.e. the circular orbital motion decreases quickly with increasing depth (Thurman and Trujillo, 2001). The wave length influences the wave base and it is equal to one half of a wave length and thus, small steepness waves are normally long waves that have a deeper wave base. The longer the wave, the faster and the longer the interaction with a sloping seabed. Many experimental, numerical, theoretical and field studies have examined the limits of the onset of wave breaking. Breaking criteria can be categorized on the basis of geometric, kinematic and dynamic breaking aspects. The geometric breaking criterion describes the limiting wave steepness in terms of wave height (H) and wave length (L), and according to Stokes (1880) wave breaking occurs when H/L reaches 0.141 and the crest angle attains 120^0. Although, when a wave gains more energy and advances breaking, then the wave crest overturns and results in an asymmetric profile both horizontally and vertically (Kjeldsen and Myrhaug, 1978). Hence, the global steepness limitation is not appropriate to characterize the onset of breaking as it does not account for the local wave profile asymmetry. Kjeldsen and Myrhaug (1978) introduced steepness and asymmetry factors to describe the geometry of breaking waves: crest front steepness (ε), crest rear steepness (δ), the vertical asymmetry factor (λ) and the horizontal asymmetry factor (μ) as defined in the Fig. 1. The kinematic criterion of wave breaking is that the crest particle velocity exceeds the wave celerity. The ratio of the crest particle velocity and the wave celerity is approximately 1.5 for plunging breakers and 1.0 for spilling breakers (Wu, 2002). From a dynamic point of view, a wave breaks when the downward acceleration at the crest exceeds half of the gravitational acceleration, and when the energy variation of high frequency waves is rapid.

Predictions of wave height and water depth at breaking and breaker types are the prominent characteristics of breaking waves used to describe the maximum hydrodynamic forces on coastal structures. The breaker depth index, γ_b describes the wave height at breaking, and is defined as the ratio of the wave height H_b and the water depth at breaking d_b:

$$\gamma_b = \frac{H_b}{d_b} \tag{1}$$

The breaker height index, Ω_b is defined as the ratio of the breaker height H_b and offshore wave height H_0:

$$\Omega_b = \frac{H_b}{H_0} \tag{2}$$

1.2 Wave profile asymmetry of shallow water waves

The degree of wave asymmetry increases as the wave propagates into shallow water and it is maximum at the breaking point. Considering the nonlinear behavior of shallow water waves, i.e. the shortening of wave length and the resulting larger wave heights, the typical values for the asymmetry profile parameters in shallow water become higher than those in deep water. A symmetrical wave propagates over a slope where it undergoes deformation (shallow water steepening) due to shoaling. The crest elevation reaches the maximum value with a decrease of trough depth, thus the wave becomes steeper but symmetric in shape. Closer to breaking, the wave starts to deform. The shape of the wave is not symmetric anymore, and the face of the wave in the crest region becomes vertical, a portion of the wave surface then overturns shoreward. Peregrine et al. (1980) investigated the changes in fluid properties during overturning in three prominent regions of a forward moving water jet: high orbital velocities

near the wave crest region, high accelerations on the forward face of the wave, and the low accelerations on the rear face of the wave.

Experimental and numerical studies have mainly focused on the characteristics of breaking waves in shallow waters based on the kinematic and dynamic evaluation of wave breaking. The geometric properties of breaking waves in shallow water was initiated by Ippen and Kulin (1954). Ippen and Kulin (1954), and later by Miller and Zeigler (1964), classified the breakers as symmetric, asymmetric and intermediate based on their deformation stage during shoaling. Adeyemo (1968) examined the effect of the beach slope and the shoaling process on wave asymmetry, categorizing the wave asymmetry with three parameters: wave vertical asymmetry, wave slope asymmetry and wave horizontal asymmetry. He tested asymmetry profile parameters of breaking wave profile over six different slopes from $1/10$ to $1/18$ and established the correlations between these asymmetry profile parameters. Iwagaki and Sakai (1972) studied experimentally and theoretically the influence of the beach slope on the change in wave height and wave asymmetry profile during breaking. They investigated the wave transformation including wave asymmetry over slopes of $1/10, 1/20$ and $1/30$. Hwang (1984) investigated the application of the wave steepness and asymmetry factors introduced by Kjeldsen and Myrhaug (1978), for shoaling waves on a mild slope in order to study the evaluation of wave asymmetry in shallow waters. In fact, there are different steepness and asymmetry factors proposed by previous studies to specify the wave profile during shoaling and breaking. However, the wave steepness and asymmetric factors proposed by Kjeldsen and Myrhaug (1978) to account for the prominent features of wave asymmetry at breaking are considered in the present study.

1.3   Environmental conditions and simulation cases

Simulation cases	Simulation no.	Surf similarity parameter, ξ	Reference water depth, d (m)	Steepness, H_0/L_0	Slope, m
Based on reference water depth (d): Case (A)	1 2 3 4 5 6	0.202	0.35 0.40 0.45 0.50 0.55 0.60	0.02	1/35
Based on offshore wave steepness (H_0/L_0): Case (B)	7 8 9 10 11 12 13 14	0.286 0.233 0.202 0.181 0.165 0.143 0.128 0.117	0.50	0.010 0.015 0.020 0.025 0.030 0.040 0.050 0.060	1/35
	15 16 17	0.471 0.283 0.202		0.02	1/15 1/25 1/35

18	0.157			1/45
19	0.128			1/55
20	0.385			1/15
21	0.231			1/25
22	0.165		0.03	1/35
23	0.128			1/45
24	0.105			1/55
25	0.333			1/15
26	0.200			1/25
27	0.143		0.04	1/35
28	0.111			1/45
29	0.091			1/55
30	0.298			1/15
31	0.179			1/25
32	0.128		0.05	1/35
33	0.099			1/45
34	0.081			1/55
35	0.272			1/15
36	0.163			1/25
37	0.116		0.06	1/35
38	0.091			1/45
39	0.074			1/55

Table 1: List of simulation cases

Numerous experimental studies have been conducted to predict the initiation of wave breaking and the breaking process. The main intention of the present simulation cases is to examine the prominent characteristics of breaking waves including the geometry of breaking waves in order to enhance the assessment of the wave breaking mechanism for different environmental conditions. The shallow water breaking wave properties including geometric properties are largely influenced by three prominent environmental parameters; the water depth, offshore steepness and beach slope. The simulation cases consist of three main cases, A, B and C as listed in Table 1. The influence of water depth (d) during breaking over a fixed slope of $1/35$ with a fixed offshore steepness of 0.02 is investigated and the wave parameters are listed in case A (A1 to A6). The intention of case B (B7 to B14) is to study the changes in wave properties with a wide range of offshore wave steepnesses (H_0/L_0) from 0.01 to 0.06 over a slope $1/35$ at d=0.5m. Finally, in order to consider the effects of seabed slopes (m) on wave breaking, five seabed slopes, $1/15$, $1/25$, $1/35$, $1/45$ and $1/55$ are examined. For each slope, steepnesses ranging from 0.02 to 0.06 at d=0.5m are simulated, as tabulated in case C (C15 to C39). In brief, a total of 39 cases covering a wide range of the three important parameters are investigated in the study.

2 Numerical Model

2.1 Governing Equations

In the present study, a 3D numerical model is employed and the RANS equations are solved together with the continuity equation for incompressible flow, prescribing mass and momentum conservation:

$$\frac{\partial U_i}{\partial x_i} = 0 \tag{3}$$

$$\frac{\partial U_i}{\partial t} + U_j \frac{\partial U_i}{\partial x_j} = -\frac{1}{\rho} \frac{\partial P}{\partial x_i} + \frac{\partial}{\partial x_j} \left[(\nu + \nu_t) \left(\frac{\partial U_i}{\partial x_j} + \frac{\partial U_j}{\partial x_i} \right) \right] + g_i \tag{4}$$

U is the velocity averaged over time t, ρ is the fluid density, P is the pressure, ν is the kinematic viscosity, ν_t is the eddy viscosity and g the acceleration of gravity term. The numerical model is used as a numerical wave tank. High-order schemes are selected for the current study to avoid unphysical damping of propagating waves. The convection term of the RANS equations is discretized with the Weighted Essentially Non-Oscillatory (WENO) scheme in the conservative finite difference version (Jiang and Shu, 1996). Here, a discretization stencil consists of three substencils, which are weighted according to the local smoothness of the discretised function. The scheme achieves a minimum of 3rd-order accuracy for discontinuous solutions, and up to 5th-order accuracy for a smooth solution. At the same time, very robust numerical stability is achieved, without the negative side effects of numerical limiters. For the time treatment, a third-order accurate total variation diminishing (TVD) Runge-Kutta scheme is employed, consisting of three Euler substeps (Shu and Osher, 1988). The pressure term is solved with the projection method (Chorin, 1968) after each of the Euler substeps for the velocities. The BiCGStab algorithm (van der Vorst H., 1992) with Jacobi scaling preconditioning solves the Poisson equation for the pressure. The RANS equations are closed with the two-equation k-ω turbulence model (Wilcox, 1994), with transport equations for the turbulent kinetic energy k and the specific dissipation ω.

2.2 Numerical Grid and Parallelization

At the solid boundaries of the fluid domain a ghost cell immersed boundary method is employed. In this method, the solution is analytically continued through the solid boundary by updating fictitious ghost cells in the solid region through extrapolation. This way, the numerical discretization does not need to account for the boundary conditions explicitly. The algorithm is based upon the local directional approach by Berthelsen and Faltinsen (2008). With this method, complex geometries and cut cells can be accounted for. The ghost cell approach has several advantages: Grid generation becomes trivial, the numerical stability and the order of the overall scheme is not affected. In addition, the method integrates well into the domain decomposition strategy for the parallelization of the numerical model. Here ghost cells are used to update the values from the neighbouring processors via MPI (Message Passing Interface).

2.3 Level Set Method

The main feature of breaking waves is the complex motion of the free surface. In order to account for this, the interface-capturing level set method is employed, describing the interface between the two phases water and air. With the level set method (Osher and Sethian, 1988), the location of the interface is represented implicitly by the zero level set of the smooth signed distance function $\phi(\vec{x}, t)$. In every point of the computational domain, the level set function gives the closest distance to the interface and the phases are distinguished by the change of the sign. This results in the following properties:

$$\phi(\vec{x}, t) \begin{cases} > 0 \ if \ \vec{x} \in water \\ = 0 \ if \ \vec{x} \in \Gamma \\ < 0 \ if \ \vec{x} \in air \end{cases} \tag{5}$$

Also the Eikonal equation $|\nabla \phi| = 1$ is valid. When the interface is moved under an externally generated velocity field $\vec{v}$, a convection equation for the level set function is obtained:

$$\frac{\partial \phi}{\partial t} + U_j \frac{\partial \phi}{\partial x_j} = 0 \tag{6}$$

With the level set function in place, the material properties of the two phases can be defined for the whole domain. Without special treatment, there is a jump in the density ρ and the viscosity ν across the interface, which can lead to numerical instabilities. This is avoided by smoothing the material properties in the region around the interface with a regularized Heavyside function $H(\phi)$. This region is 2ϵ thick, with ϵ being proportional to the grid spacing Δx. In the present paper it was chosen to be $\epsilon = 1.6\Delta x$. The density and the viscosity can then be written as:

$$\begin{aligned} \rho(\phi) &= \rho_{water} H(\phi) + \rho_{air} (1 - H(\phi)), \\ \nu(\phi) &= \nu_{water} H(\phi) + \nu_{air} (1 - H(\phi)) \end{aligned} \tag{7}$$

and the regularized Heavyside function:

$$H(\phi) = \begin{cases} 0 & if \ \phi < -\epsilon \\ \frac{1}{2} \left(1 + \frac{\phi}{\epsilon} + \frac{1}{\Pi} sin \left(\frac{\Pi \phi}{\epsilon} \right) \right) & if \ |\phi| < \epsilon \\ 1 & if \ \phi > \epsilon \end{cases} \tag{8}$$

2.4 Numerical Wave Tank

A numerical wave tank needs to generate waves at the inlet boundary and absorb waves at the outlet boundary in order to simulate the flow and free surface dynamics of a wave flume. In the present numerical model, the relaxation method is selected for the generation and absorption of waves. The relaxation method concept was first presented by Larsen and Dancy (1983), where the analytical solution is used to moderate the computationally generated waves. This method has been presented by Mayer et al. (1998) and Engsig-Karup (2006). The relaxation function presented by Jacobsen et al. (2012) is used in the present study. In the wave generation relaxation zone, the values for the velocities and the free surface are ramped up from the

computational values to the the values obtained by wave theory. This generates high quality waves and reflections traveling towards the generation zone are effectively absorbed. In the numerical beach relaxation zone, the computational values for the velocities are smoothly reduced to zero, the free surface modulated to the still water level and the pressure to the according hydrostatic distribution. In the current case of the sloping beach, the relaxation zone for the numerical beach is not employed.

3 Results and Discussion

3.1 Comparison of experimental measurements and numerical model results

3.1.1 Computational set-up
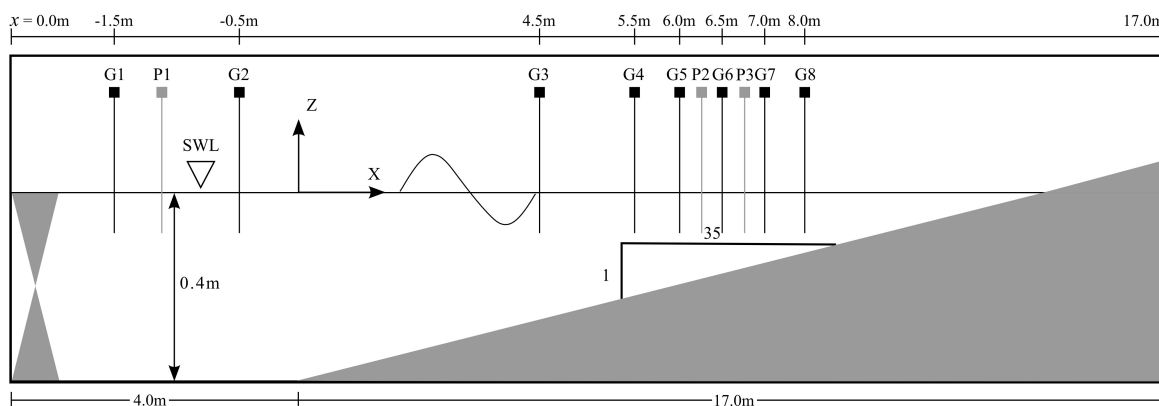
Figure 2: Computational set-up: G1-G8 are wave gauge positions and P1-P3 are velocity probe positions

The numerical experiment of breaking waves on a sloping bed is carried out in the numerical wave tank in a 2D setting, allowing for more computationally efficient simulations. To verify the performance of the numerical model, the simulated results are compared with the experimental data for the spilling breaker case from the physical model test reported by Ting and Kirby (1994). The present numerical set up and the wave parameters resemble the experimental conditions given by Ting and Kirby (1994). The numerical wave tank consists of a 4m long horizontal bed with the constant water depth of 0.4m, followed by a slope 1/35 as shown in the Fig. 2. The coordinate system is the same as in the experimental study. The water surface elevation and the kinematics in the wave generation zone are specified using the 5th-order Cnoidal wave theory presented by Fenton (1999). The incident wave height and period of the Cnoidal waves are $H = 0.125m$ and $T = 2.0s$ in the horizontal bed region. The instantaneous free surface elevations and horizontal velocities are calculated using wave gauges and velocity probes at several locations identical with the experimental positions along the wave tank. The computational domain is discretized with a uniform grid size in both directions x and y. The length of the simulation in the present study is 25s in order to achieve a quasi-steady state for the mean quantities and the mean wave quantities are calculated from

the last five waves.

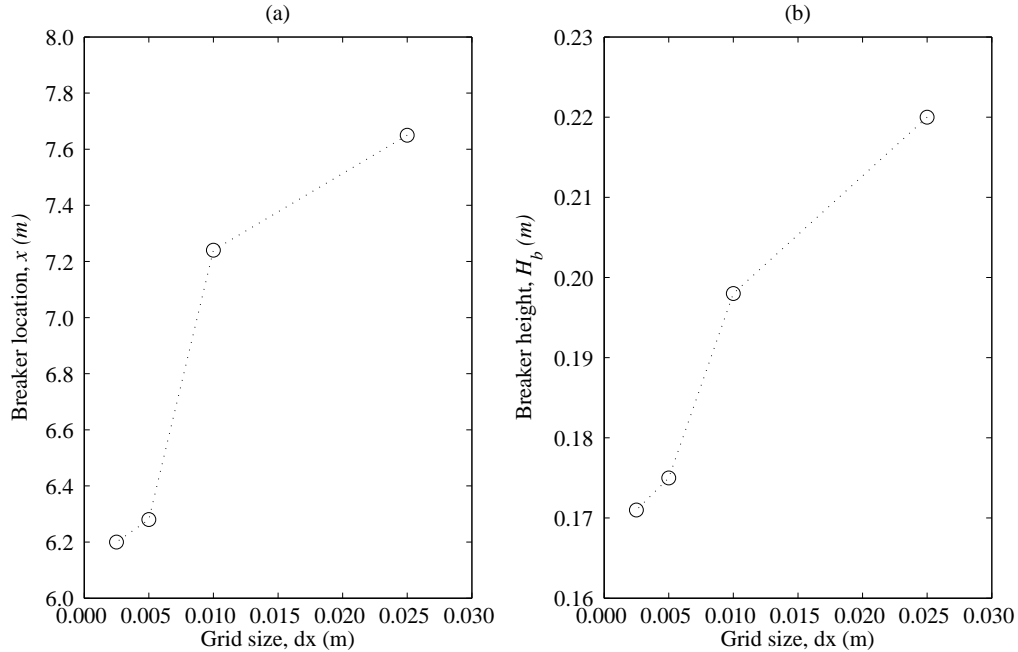### 3.1.2 Grid refinement study

Figure 3: Grid refinement study on simulated results (a) breaker location (x)and (b) breaker height (H_b)

The effect of the grid size on the numerical simulation of breaking waves are investigated with four different grid sizes dx=0.025m, dx=0.01m, dx=0.005m and dx=0.0025m. The breaking location and the breaker height are considered to examine the grid convergence through comparison with the experimental breaking location, x_b=6.4m and breaker height, H_b=0.163m as shown in Fig. 3 (a) and (b), respectively. On coarser grid sizes dx=0.025m and dx=0.01m, the wave breaks later shoreward with higher breaker height than in the experiments. Although the results of the finer grids are in good agreement with the experimental data at the breaking point, the grid size dx=0.005m with 808614-number of grid cells is chosen for the present study since the difference between 0.0025m and 0.005m is negligible as shown in Fig. 3 and the computational time is extremely high for the dx=0.0025m with 3234513-number of grid cells.

3.1.3 Wave breaking over a sloping bed
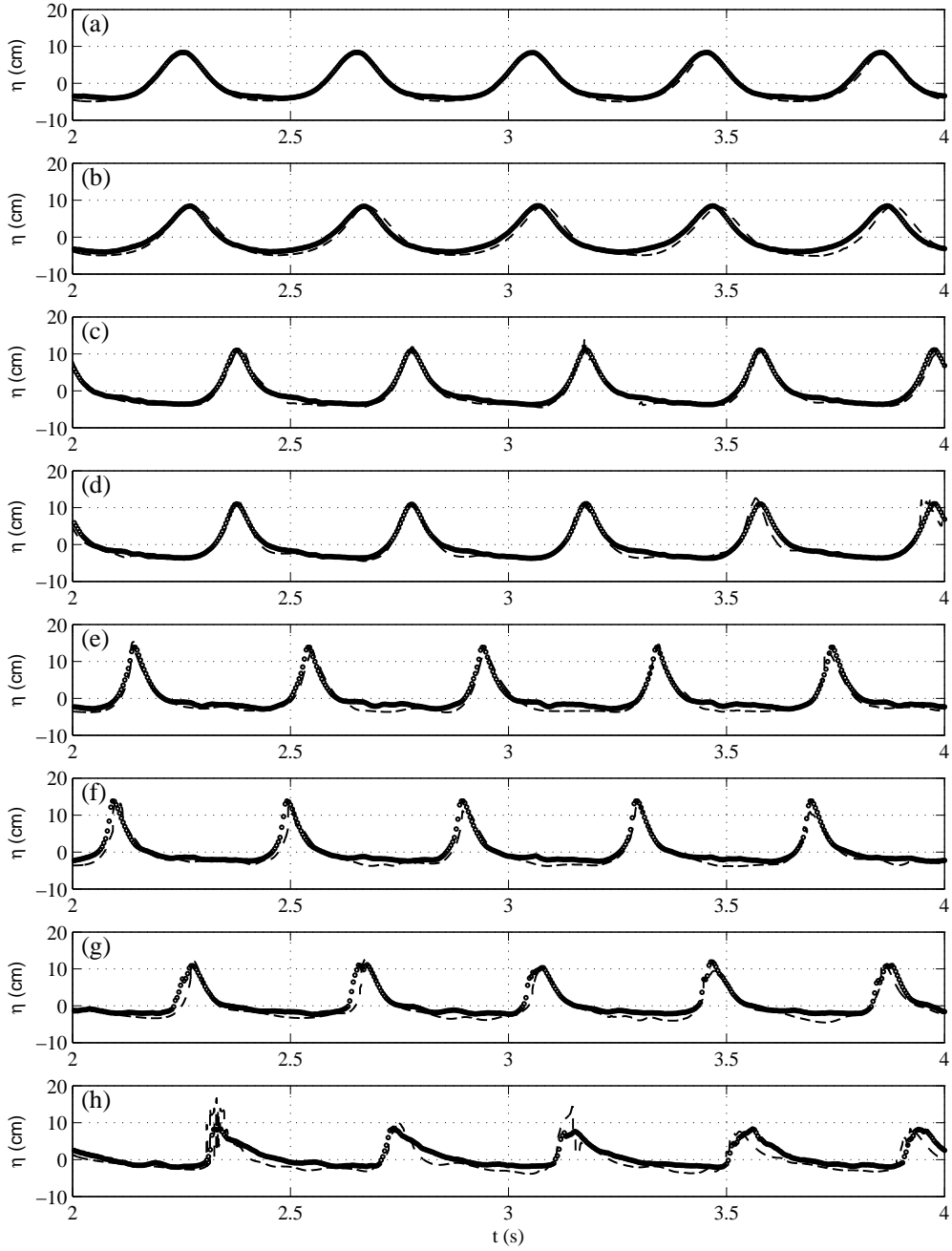
Figure 4: Comparison of computed and measured water surface elevations for spilling breaker case at $x=$ -1.5m, -0.5m, 4.5m, 5.5, 6.0m, 6.5m, 7.0m and 8.0m. Dashed lines: present numerical model; circles/full line: experimental data from Ting and Kirby(1996)

The simulated results are compared with the experimental measurements for spilling breakers. The comparison of simulated and measured instantaneous free surface elevations for eight wave gauges along the wave tank is shown in Fig. 4. The eight wave gauges (G1-G8) are positioned at x= -1.5m, -0.5m, 4.5m, 5.5m, 6.0m, 6.5m, 7.0m and 8.0m from the toe of the slope (see Fig. 1) to evaluate the performance of the numerical model on predicting the complete wave transformation process from wave generation, shoaling and onset of wave breaking to post-breaking.

It is observed that the wave height increases and the trough flattens as the wave advances over the sloping bed. In fact, the crest becomes shorter and steeper and the trough becomes longer and flatter as the water depth decreases in order to maintain the constant energy flux during the shoaling process. Further, the momentum and energy in the vicinity of the wave crest increase as the shoaling proceeds until the wave crest reaches a maximum height and the wave front becomes almost vertical and eventually breaks at x_b=6.28m. Thus, the numerical waves break at almost the same location as the experimental waves at x_b=6.4m. Finally, the wave height decreases after breaking as the waves propagate further over the slope. The simulated free surface elevations exhibit the typical behavior of the Cnoidal waves on sloping beds (non-linear shallow water waves). Moreover, the numerical prediction of free surface elevations are also in good agreement with the experimental measurements in all the regions from the wave generation region to the post-breaking region.
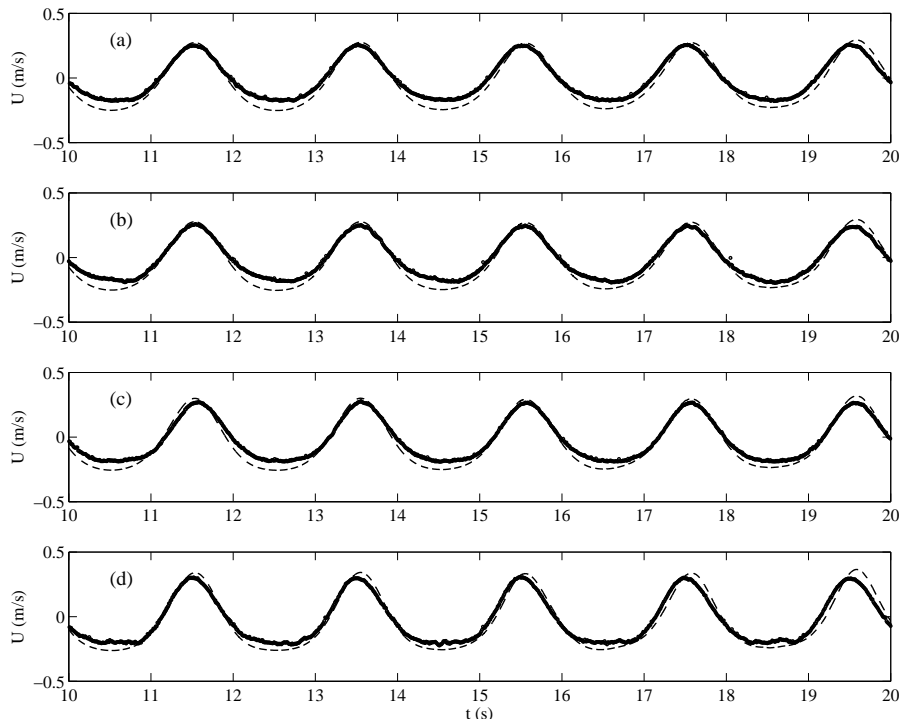

Figure 5: Comparison of computed and measured horizontal velocities for spilling breaker case at x=-1.265m and z=-0.36m (a), -0.30m (b), -0.20m (c) and -0.10m (d). Dashed lines: present numerical model; circles/full line: experimental data from Ting and Kirby(1996)

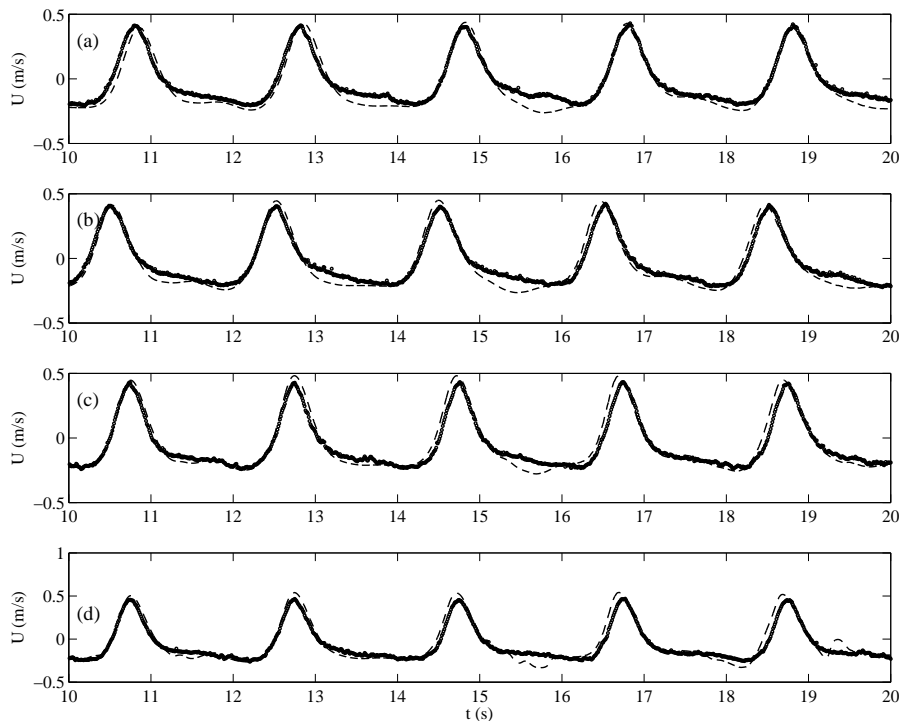The horizontal velocity variations over depth are measured using velocity probes at three

Figure 6: Comparison of computed and measured horizontal velocities for spilling breaker case at x=5.945m and z=-0.18m (a), -0.15m (b), -0.10m (c) and -0.05m (d). Dashed lines: present numerical model; circles/full line: experimental data from Ting and Kirby(1996)

different locations (P1-P3): in the wave generation region (x=-1.265m), before (x=5.945m) and after (x=6.665m) breaking are shown in Figs. 5, 6 and 7 respectively. It is observed that the horizontal velocities are higher in the vicinity of the wave crest near the free surface (Fig. 5 (a)) and decrease away from the free surface (Fig. 5 (d)). Fig. 7 shows that the computed horizontal velocities at x=6.665m are in the post breaking region. The crest velocities agree well with the experimental data, but some short downspikes are observed in the trough region. The reason for the short downspikes in the trough portion is unclear but this might be related to the interaction of active turbulence with air entrainment which affects the dissipation of energy in the surf zone. As the main intention of the study is to investigate the effect of environmental parameters on breaking characteristics, the air entrainment and associated processes are not investigated in details further. Moreover, during breaking the large fluid flow structures degenerate into smaller flow structures with air entrainment and extreme turbulent behaviour. It is therefore intricate to measure and calculate the horizontal velocity in this region. Moreover, the velocities increase as the wave approaches the slope until breaking as shown in Fig. 6 (a) and Fig. 7 (a). Overall, the wave height and the velocity increase and the wave length decreases as the waves shoal over the slope, thus a further increase in the wave height causes the fluid particles to move faster than the wave celerity and eventually breaking occurs. From the simulated results it is evident that the present numerical model is able to predict the trend of the horizontal velocity variation versus the depth and the tank length quite well. The simulation results are also consistent with the experimental results.
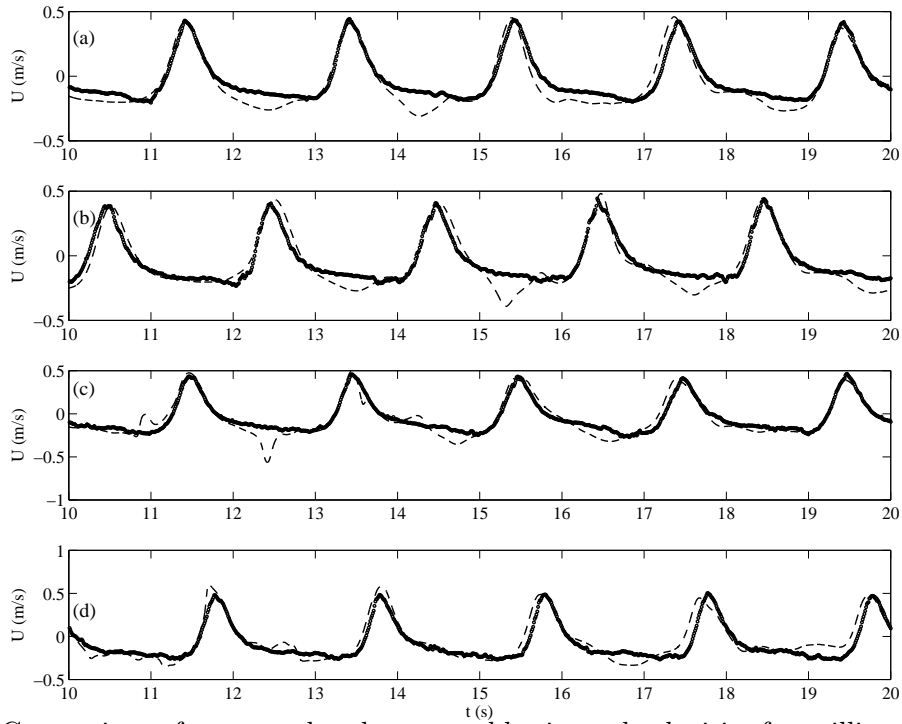
Figure 7: Comparison of computed and measured horizontal velocities for spilling breaker case at x=6.665m and z=-0.17m (a), -0.15m (b), -0.10m (c) and -0.05m (d). Dashed lines: present numerical model; circles/full line: experimental data from Ting and Kirby(1996)
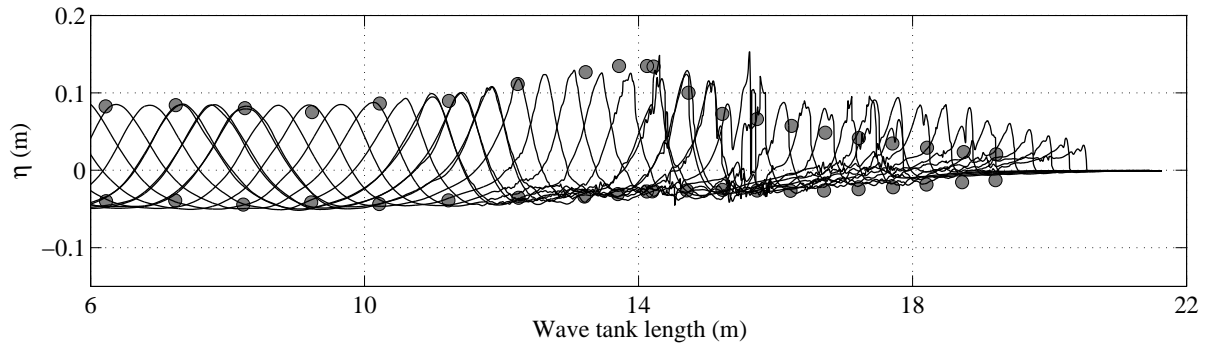

Figure 8: Comparison of computed and measured envelope of water surface elevation for spilling breaker case. Solid lines: the present numerical model; circles: experimental data from Ting and Kirby(1996)

Fig. 8 shows comparison of the measured and simulated distribution of wave amplitudes. The wave height increases as the waves traverse over the slope until breaking occurs, and the wave height diminishes shoreward after breaking. The wave height reaches the maximum before breaking and the waves break at x_b=6.28m; thus the numerical waves break close to the measured breaking point at x_b=6.4m. Moreover, the present model yields a good prediction of shoaling wave heights, wave crest and trough heights in the breaker zone (before breaking and at breaking). In the surf zone, the present model slightly overestimates the wave crest but yields a good prediction of the wave troughs. The reason for the over-prediction of the wave crest in the surf zone is not clear, though it might be related to the slower numerical dissipation of energy than in the experiments.

3.1.4 Breaking process

Fig. 9 presents the change in the wave surface profile and the velocity distribution near the breaking region at different stages of the breaking process. The velocity of the displacement of fluid particles in the wave depends on the wave amplitude. The sequence of the breaking process evolution depicts the mixing of air and water and the return velocity from the slope during breaking. It is noticed that the onset of wave breaking is associated with a small water jet at the wave crest for spilling breakers. As presented in the section 3.1.3, the particle velocity increases near the wave crest as the wave propagates over the slope and the wave celerity is reduced. When the wave advances over the slope, it becomes higher due to shoaling; the potential energy increases and accordingly, the wave crest particle velocity. When the crest particle velocity exceeds the wave celerity, leading to an overturning motion of the wave crest with the forward ejection of a small scale water jet similar to that developed for a plunging breaker. The simulated topological features of spilling breakers are consistent with those of other studies (Lubin et al., 2011; Lader, 2002; Duncan, 2001). In fact, the particles close to crest with higher amplitudes propagate faster, thus the steepness of the wave is enhanced and the wave profile is continuously deformed. At a certain point the wave crest falls down and hits the water surface with the forward wave front enclosing a pocket of air as shown in Fig. 9(f), the so-called splash-up phenomenon. Consequently, the impact of the jet with a pocket of air on the surface generates another forward upstream jet with a cavity of air as seen in Fig. 9(g), thus drastic flow circulation is created immediately.

Fig. 10 presents the vertical variation of the velocity over the depth with maximum velocity at the wave crest front and changes in the velocity at the wave crest during breaking. The velocity profile close to wave crest becomes wider as the water jet grows faster. It can be seen from Figs. 9 and 10, that initially the particle velocities at the interface are almost equal and directed horizontally. As the wave grows further, the particles with higher velocities move forward with the ejected wave front. It is also observed, that the particle velocities are higher in the breaking region. The velocity vectors are focused close to the wave crest and thus, a portion of the wave crest that has higher velocities overturns and impinges the water surface. A topology induced vorticity is created and the jet impingement modifies the flow pattern, which is responsible for the production of turbulence and vorticity at the free surface. The numerical model can simulate the flow pattern during wave breaking including the displacement of the air pocket as shown in Fig. 10.
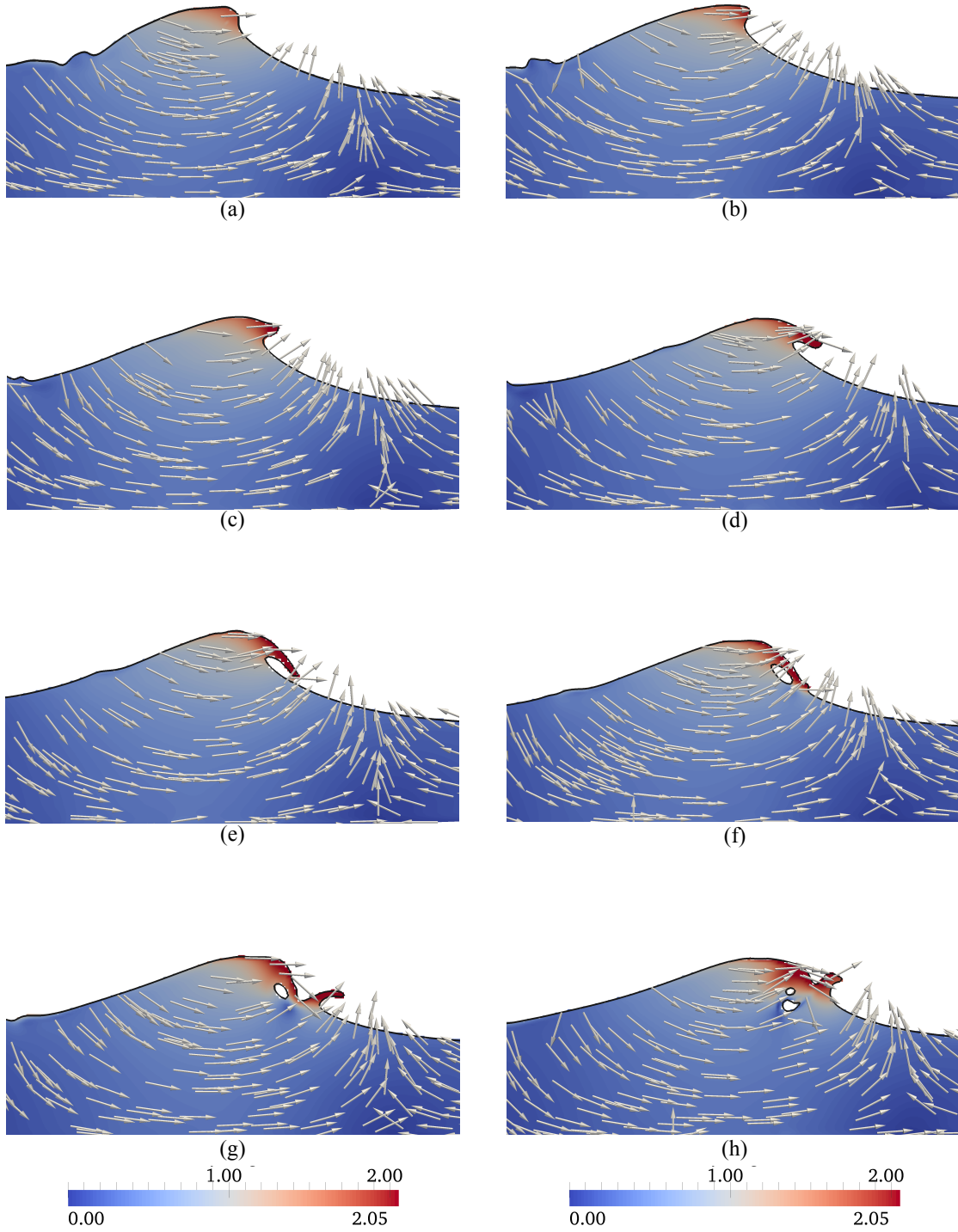
Figure 9: Computed wave profile with the velocity (m/s) variation during the wave breaking process of the spilling breaker (from (a) to (h))
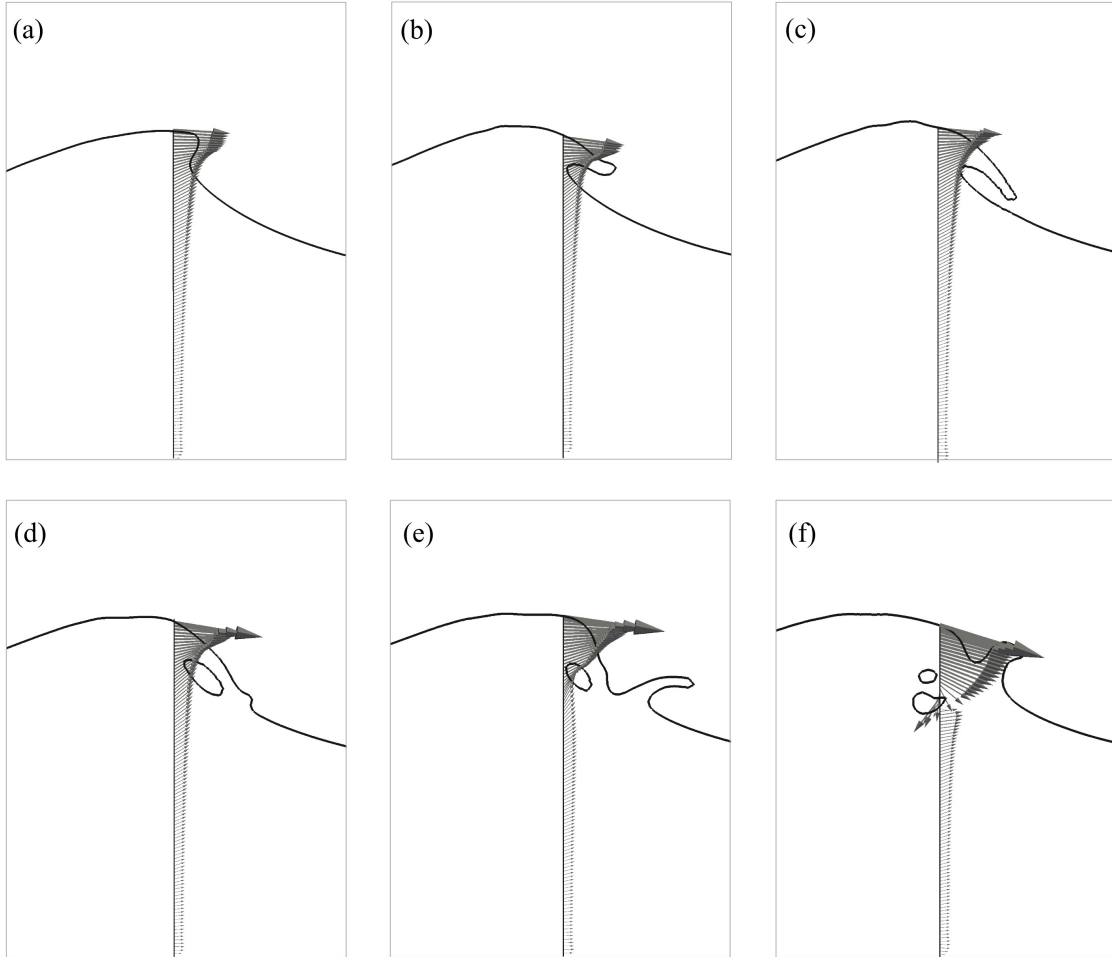
Figure 10: Computed velocity profile during the wave breaking process of the spilling breaker (from (a) to (f))

3.2 Prediction of breaking wave characteristics

As presented in Section 1.3, simulations are performed for the runs given in Table 1. Incipient breaking can be defined based on kinematic, geometric and dynamic breaking criteria. However, there are two breaking conditions that are considered for spilling breakers in the study. Firstly, the breaking point is defined as the point where most of the wave front becomes vertical, and secondly, the point where the water starts falling down at the wave front. The assessment of the breaker height, water depth at breaking, location of breaking point and wave steepness and asymmetry factors are indicated in Fig. 1. The breaker location (x) is measured from the toe of the slope and the breaker water depth d_b is measured from the still water level at which wave breaking occurs.

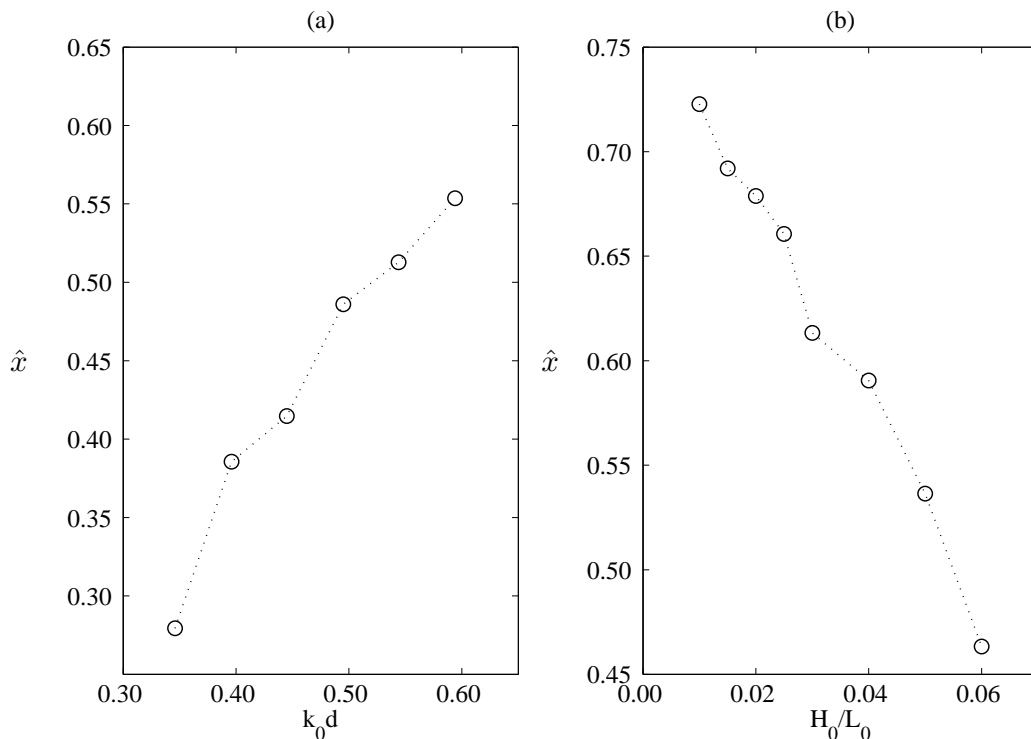### 3.2.1 Onset of wave breaking

Figure 11: Computed non-dimensional breaker location ($\hat{x}$) as a function of (a) non-dimensional water depth ($k_0 d$) and (b) offshore wave steepness (H_0/L_0)

The breaker location is presented in the non-dimensional form, $\hat{x} = x/L$ from the toe of the slope ($x = 0$) to the end of the slope ($x = L$). Figs. 11 (a) and 12 (a) present the non-dimensional breaker location ($\hat{x}$) and the non-dimensional breaker depth (d_b/d), respectively, versus the non-dimensional water depth ($k_0 d$). It appears that $\hat{x}$ increases and d_b/d decreases almost linearly as $k_0 d$ increases for cases A1 to A7 (see Table 1), i.e. the shallower the reference water depth (d), the larger the breaker water depth (d_b). This implies that the wave profile has sufficient time to alter the equilibrium profile to the proximity water depth. Moreover, it deforms later as d increases. A wave with a given offshore steepness (H_0/L_0) breaks further shoreward as d increases (case A6), corresponding to d_b/d=0.350, $k_0 d$=0.595 in Fig. 12 (a). Figs. 11 (b) and 12 (b) show the non-dimensional breaker location ($\hat{x}$) and the breaker depth (d_b/d), respectively, versus the offshore steepness (H_0/L_0). It appears that $\hat{x}$ decreases and d_b/d increases as H_0/L_0 increases for cases B7 to B14. When a wave advances over a given slope and reference water depth, the height of the wave increases and the length of the wave decreases as the wave shoals and consequently, a small increase in wave height causes waves with larger H_0/L_0 to reach the breaking point sooner than waves with small H_0/L_0. Hence, x moves shoreward and d_b becomes shallower as H_0/L_0 decreases.

Fig. 13 shows $\hat{x}$ versus the surf similarity parameter ($\xi = \frac{m}{\sqrt{H_0/L_0}}$) for different slopes (cases C15-C39). It appears that $\hat{x}$ increases as ξ increases for a given slope, and that the $\hat{x}$
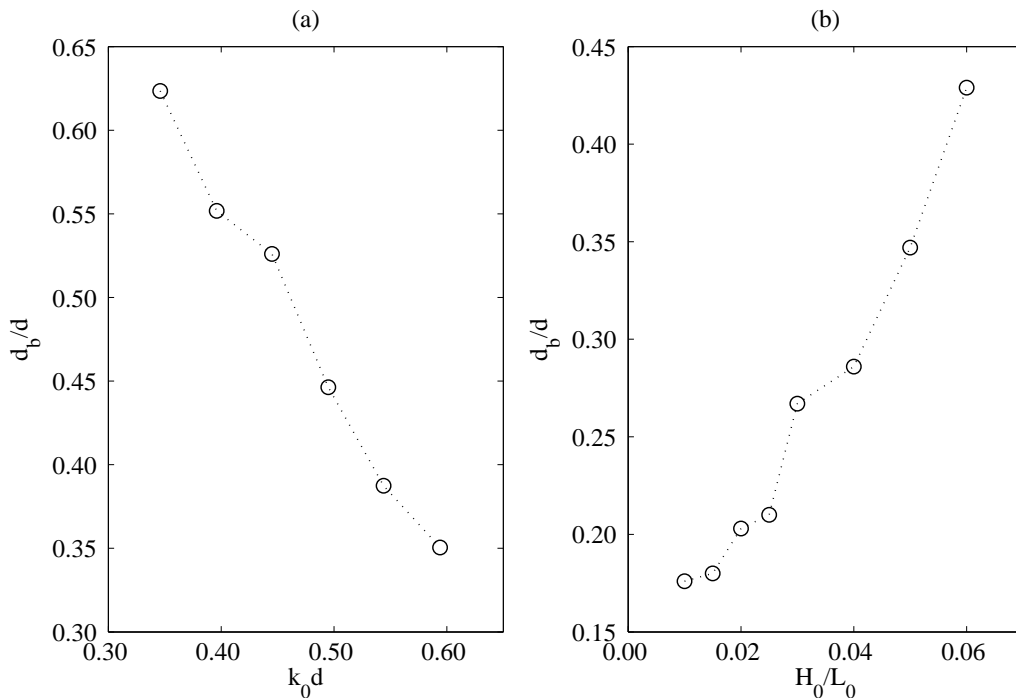
Figure 12: Computed relative water depth at breaking (d_b/d) as a function of (a) non-dimensional water depth (k_0d) and (b) offshore wave steepness (H_0/L_0)

versus ξ dependence decreases as the slope increases. The wave shoaling distance over steep slopes is shorter than on milder slopes due to the wave base effect, implying that significant partial reflection from the steep slope during shoaling causes wave breaking earlier on steeper slopes (Grilli et al., 1995; Tsai et al., 2005). Moreover, the reflection coefficient of waves on sloping sea beds can be calculated using an empirical formula proposed by Battjes (1974):

$$K_r = 0.1\xi \qquad (9)$$

where K_r is the reflection coefficient. It is noticed from the above equation that long waves would experience more reflection than short waves. Although waves are reflected from the beach, this does not mean that all of the wave energy is reflected back, hence partially reflected waves may contribute to amplify the incident wave height, depending on the period and phase of the reflected wave. Hence, wave reflection and the effect of reflection increase with steeper seabed slopes, as studied experimentally and theoretically by Tsai et al. (2005).

Fig. 14 presents d_b/d versus ξ for different slopes. It appears that d_b/d decreases as ξ increases, and that the d_b/d versus ξ dependence decreases as the slope increases. This also means that d_b/d increases with slopes for H_0/L_0 =0.02 to 0.04 (cases C15 to C29) and that d_b/d decreases with slopes with for H_0/L_0 =0.05 and 0.06 (cases C30 to C39). A possible explanation for this might be that the partial wave reflection and shoaling effect increase with the slope for H_0/L_0=0.02 to 0.04 and these effects enhance the steepening of the local wave slope, therefore waves break offshore at higher d_b over steeper slopes. In the case of H_0/L_0=0.05 and 0.06, the wave shoaling rate is higher for milder slopes and thus the wave
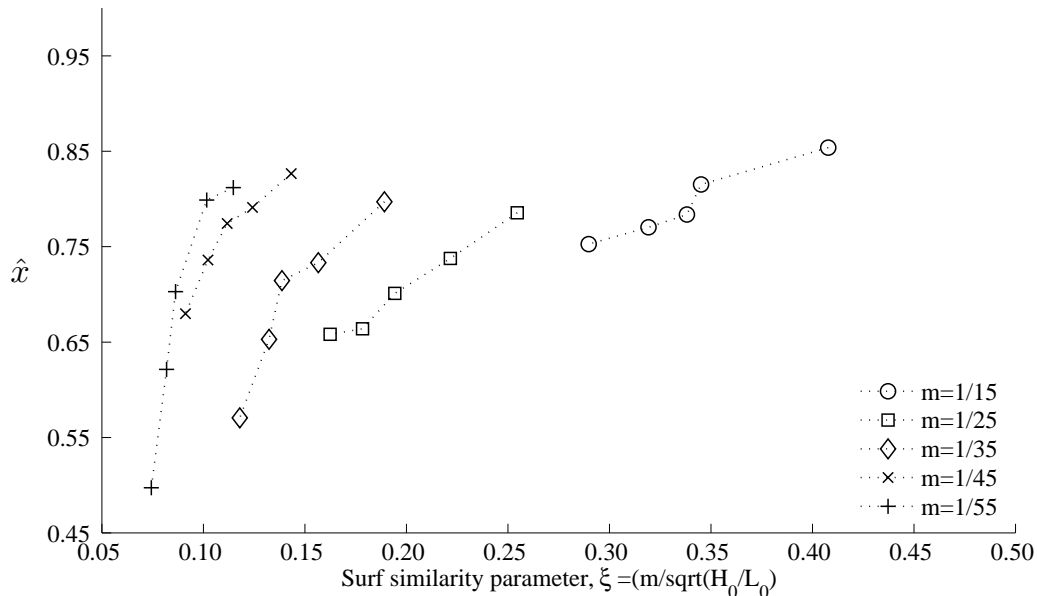
Figure 13: Computed non-dimensional breaker location ($\hat{x}$) as a function of surf similarity parameter (ξ) for different slopes

breaks sooner. Therefore it is possible that waves with larger H_0/L_0 break earlier at higher d_b on milder slopes. This is in agreement with the theoretical study by Iwagaki and Sakai (1972) and the numerical study by Grilli and Horrillo (1997). They reported that the shoaling rate is lower for steeper slopes than for milder slopes. On steeper slopes, the wave height does not change much under shoaling, until the wave experiences the partial wave reflection from the slope, resulting in a delay of wave breaking.

3.2.2   Breaker depth index (γ_b) and breaker height index (Ω_b)

The breaker height (H_b) and the water depth at breaking (d_b) are calculated from the numerical evaluation of the wave surface elevation. Fig. 15 (a) shows the breaker depth index ($\gamma_b = H_b/d_b$) and the breaker height index ($\Omega_b = H_b/H_0$) versus the non-dimensional water depth (k_0d)(cases A1 to A6). It appears that γ_b and Ω_b reduce as d increases. For a given offshore steepness and slope, H_b decreases as the wave shoals for larger reference water depth (d). Thus, these results suggest that waves advancing over shallower d experience more shoaling and break sooner at larger d_b, corresponding to $\hat{x}$=0.280, k_0d=0.34 in Fig. 11 (a) and d_b/d=0.62, k_0d=0.34 in Fig. 12 (a). The prediction of this non-linear behavior of waves is also reported in the study by Iwagaki and Sakai (1972). Moreover, the wave celerity is directly proportional to the square root of the water depth in shallow water. Another possible explanation for this is that a wave propagating from larger d, needs to propagate further shoreward until the breaking point at which the orbital velocity overcomes the celerity of the wave.

Fig. 15 (b) shows the breaker depth index (γ_b) and the breaker height index (Ω_b) versus H_0/L_0 (cases B7 to B14). It appears that γ_b and Ω_b decrease with increasing H_0/L_0. The reduction in H_b with increasing H_0/L_0 shows that the wave with larger H_0/L_0 advancing over
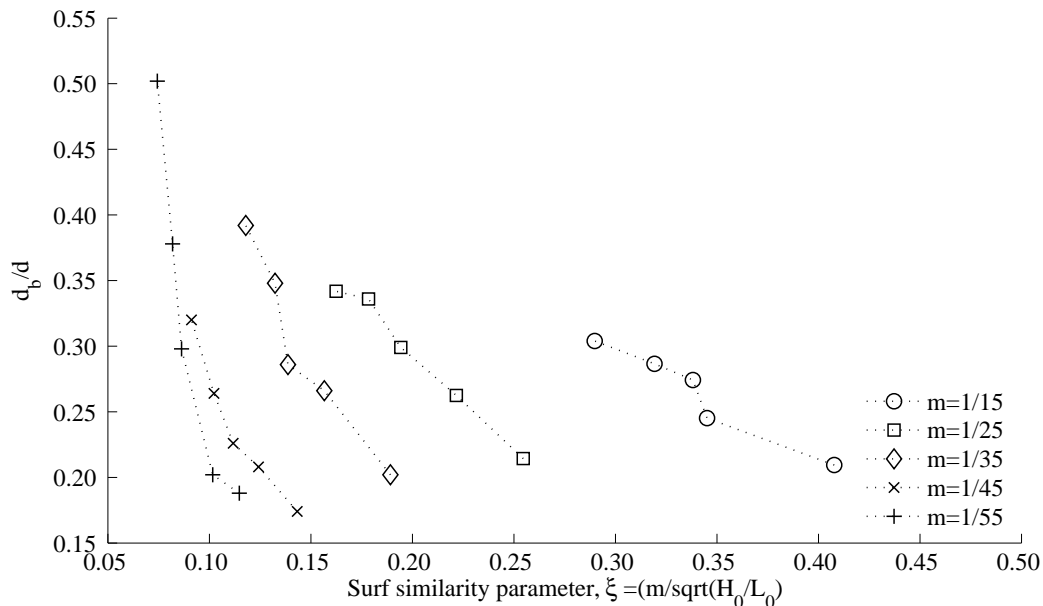
21

Figure 14: Computed relative water depth at breaking (d_b/d) as a function of surf similarity parameter (ξ) for different slopes

a slope breaks earlier (i.e. further offshore) during shoaling at larger d_b, corresponding to case B14, $\hat{x}$=0.46, H_0/L_0=0.06 in Fig. 11 (b) and d_b/d=0.43, H_0/L_0=0.06 in Fig. 12 (b). In the same way, waves with low H_0/L_0 waves propagate further up on the slope and break at shallower d_b corresponding to case B7, $\hat{x}$=0.72, H_0/L_0=0.01 in Fig. 11 (b) and d_b/d=0.17, H_0/L_0=0.01 in Fig. 12 (b). This is consistent with the study by Grilli et al. (1995).

Figs. 16 and 17 present the breaker depth index (γ_b) and breaker height index (Ω_b), respectively, versus the surf similarity parameter (ξ) for different slopes. Overall it appears that γ_b and Ω_b increase as ξ increases for a given slope. This also means that at a given water depth, γ_b decreases and Ω_b increases with slopes for H_0/L_0=0.02 to 0.04 (cases C15 to C29) and γ_b increases and Ω_b decreases with slopes for H_0/L_0=0.05 and 0.06 (cases C30 to C39). Thus these results suggest that the waves break further shoreward at shallower d_b with an increase in H_b under shoaling, resulting in higher γ_b on milder slopes, i.e. corresponding to case C19, ξ=0.128 and $\hat{x}$=0.81 (Fig. 13), d_b/d=0.19 (Fig.14), γ_b=1.29 (Fig. 16), Ω_b=1.25 (Fig. 17). This variation over milder slopes suggests that the smaller the offshore wave steepness, the larger the deformation. This is consistent with the numerical study on breaking characteristics for solitary waves on slopes by Grilli and Horrillo (1997). It seems that the increase of Ω_b with steeper slopes is due to the effect of partial reflection being more pronounced on steeper slopes during shoaling. The waves with larger H_0/L_0 on milder slopes undergo higher shoaling and experience almost no reflection, thus higher γ_b and d_b/d are obtained than for waves on steeper slopes, corresponding to case C39 (ξ=0.074, Ω_b=1.0, d_b/d=0.5; Fig. 17) and C35 (ξ=0.272, Ω_b=0.879, d_b/d=0.32; Fig. 14). Moreover, the results suggest that the breaker depth index (γ_b) is more influenced by the water depth at breaking (d_b) than by the breaker height (H_b). Interestingly, the variation of H_b on slopes is mainly influenced by wave shoaling on milder
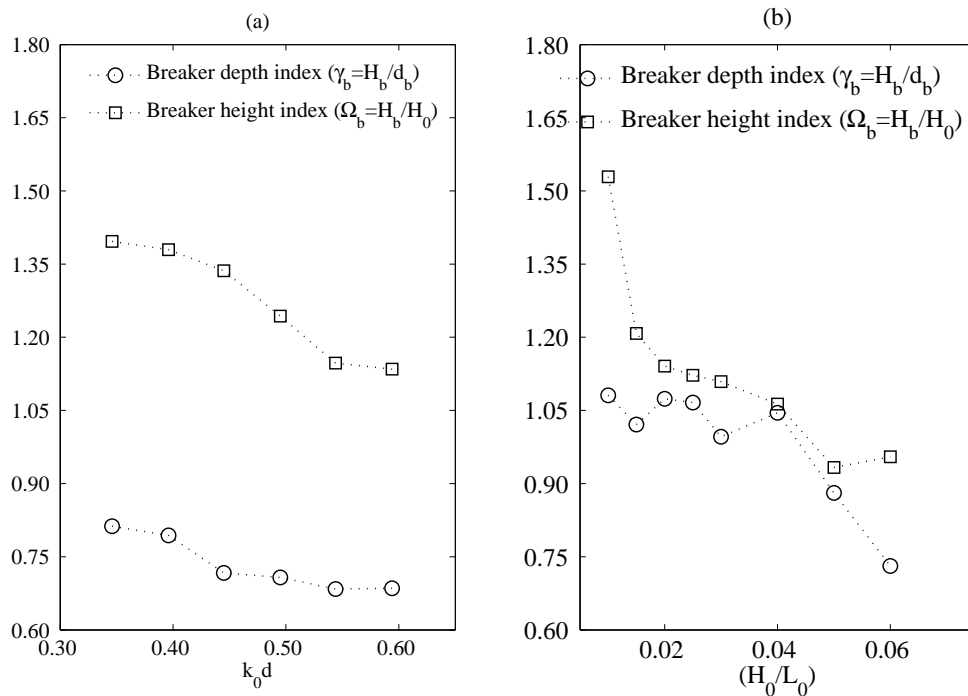
Figure 15: Breaker depth index (γ_b) and breaker height index (Ω_b) as a function of (a) non-dimensional water depth (k_0d) and (b) offshore wave steepness (H_0/L_0)

slopes and by partial reflections on steeper slopes. It is therefore reasonable to consider the combined effect of shoaling and partial reflections on breaking over steep slopes. To the present authors knowledge no data exist in the open literature on the behavior of waves on different slopes. Although previous studies have reported partial reflection on steeper slopes (Tsai et al., 2005; Grilli et al., 1995; Walker and Headland, 1982; Schultz et al., 2006), this effect has not been described based on the relationship between H_0/L_0 and H_b over moderate slopes.

3.2.3   Geometric properties of breaking waves

The steepness and asymmetry factors introduced by Kjeldsen and Myrhaug (1978) defined in Fig. 1 are used to describe wave asymmetry at the onset of wave breaking. Fig. 18 shows the crest front steepness (ε), the crest rear steepness (δ), the horizontal asymmetry factor (μ) and the vertical asymmetry factor (λ) versus the non-dimensional water depth (k_0d). It appears that ε, λ and μ increase whereas δ decreases with increasing k_0d. It is observed that the dependence of μ on k_0d seems to be very weak. Thus, waves from larger d propagates further up the slope and reach the breaking point at smaller d_b with steeper crest, corresponding to k_0d=0.59 (case A6), and $\hat{x}$=0.56 (Fig. 11 (a)), d_b/d=0.35 (Fig. 12 (a)), ε=0.79 (Fig. 18 (a)) and λ=3.5 (Fig. 18 (b)). This implies that the wave front becomes vertical, overturns and ejects forward at the breaking point as the reference water depth increases. Accordingly, the degree of asymmetry increases with increasing water depth.
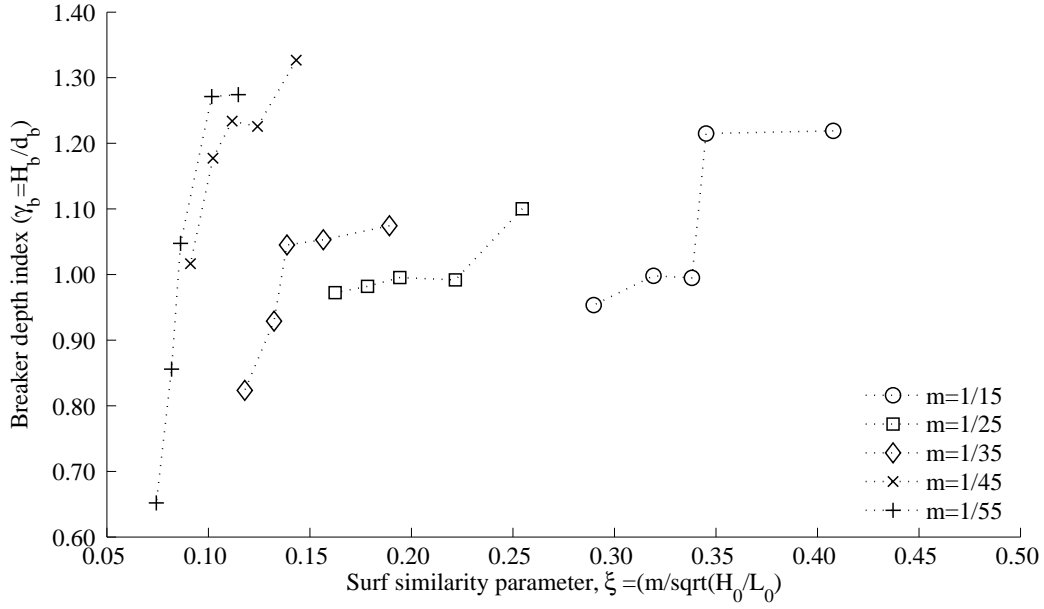
23

Figure 16: Breaker depth index (γ_b) as a function of surf similarity parameter (ξ)for different slopes
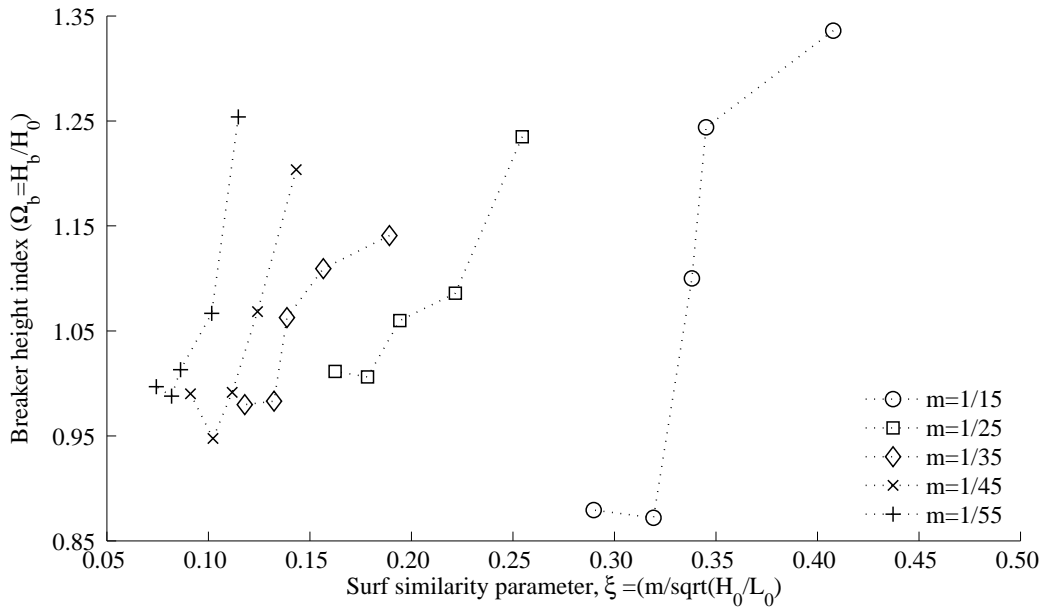

Figure 17: Breaker height index (Ω_b) as a function of surf similarity parameter (ξ) for different slopes
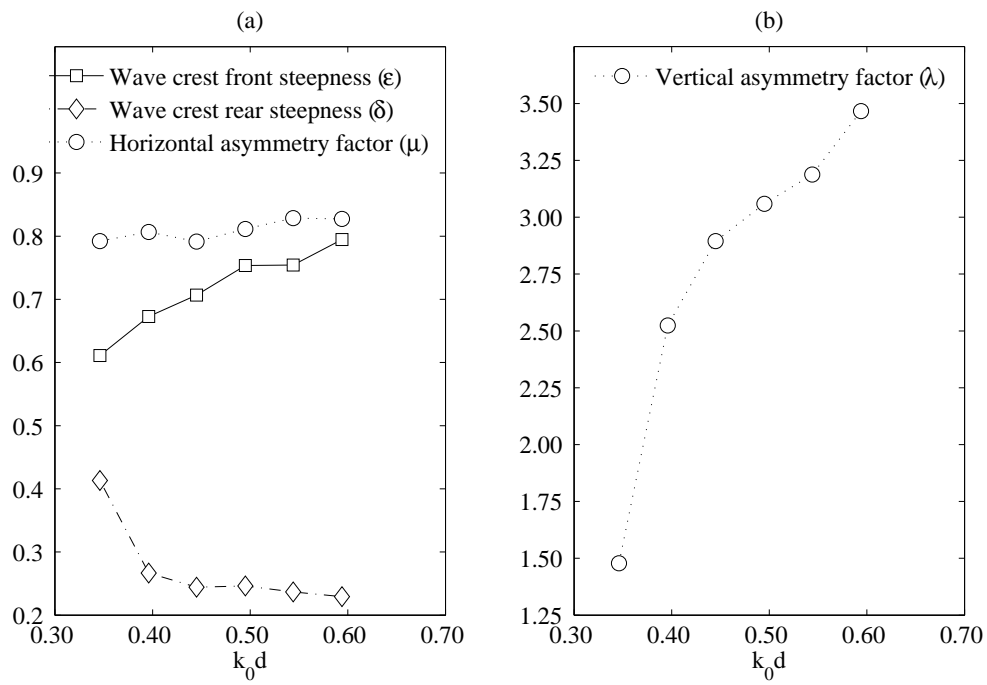
Figure 18: Computed wave steepness and asymmetry factors for different non-dimensional water depth ($k_0 d$)
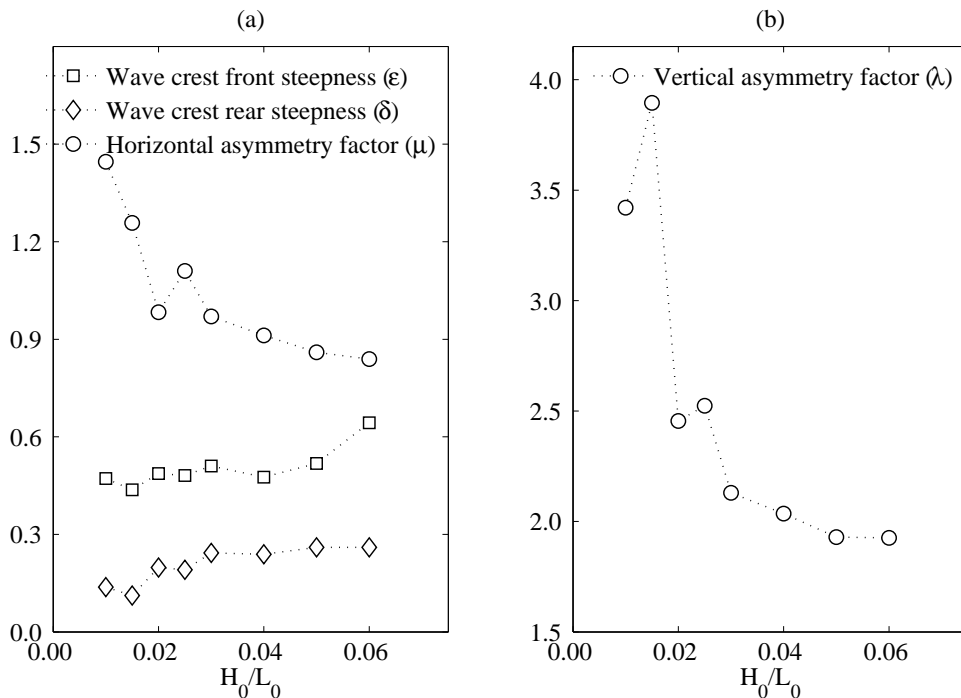
(a)

(b)

Figure 19: Computed wave steepness and asymmetry factors for different offshore wave steepness (H_0/L_0)

Fig. 19 shows the crest front steepness (ε), the crest rear steepness (δ), the horizontal asymmetry factor (μ) and the vertical asymmetry factor (λ) versus H_0/L_0. It appears that ε and δ increase whereas λ and μ decrease with increasing H_0/L_0. The results imply that waves with high H_0/L_0 propagating over a slope, do not change much from their initial geometry since they break further offshore at higher d_b with lower Ω_b, corresponding to H_0/L_0=0.06 (case B14) and $\hat{x}$=0.46 (Fig. 11 (b)), d_b/d=0.43 (Fig. 12 (b)), Ω_b=0.95 (Fig. 15 (b)). This suggests that the geometry of waves with large H_0/L_0 has a high and steep wave front and wide rear part with a lower wave trough, corresponding to ε=0.64, δ=0.27, μ=0.86 and λ=1.93 in Fig. 19. The degree of horizontal and vertical asymmetry decreases with increasing deep water steepness.

Fig. 20 shows the wave profile changes during the breaking process for different slopes. Figs. 21 and 22 show the crest front steepness (ε) and the crest rear steepness (δ), respectively, versus the surf similarity parameter (ξ) for different slopes. It appears that ε and δ decrease as ξ increases for a given slope (except for m=1/15), while for m=1/15 (cases C15, C20, C25, C30, C35), ε and δ increase as ξ increases. This is consistent with the previous results for different H_0/L_0 as shown in Fig. 19. The changes in ε and δ for m=1/15 are most probably due to partial reflections from the slope as discussed in Sections 3.2.1 and 3.2.2. Moreover, the wave with H_0/L_0=0.02 on the slope m=1/15 (case C15) has the highest value of Ω_b, corresponding to ξ=0.47, Ω_b=1.33 in Fig. 17. The surf similarity parameter of case C15 is 0.47, which is very close to the plunging breaker value of 0.5. Additionally, the wave profile geometry of case C15 also looks more like a plunging breaker, as presented in Fig. 20(c). This
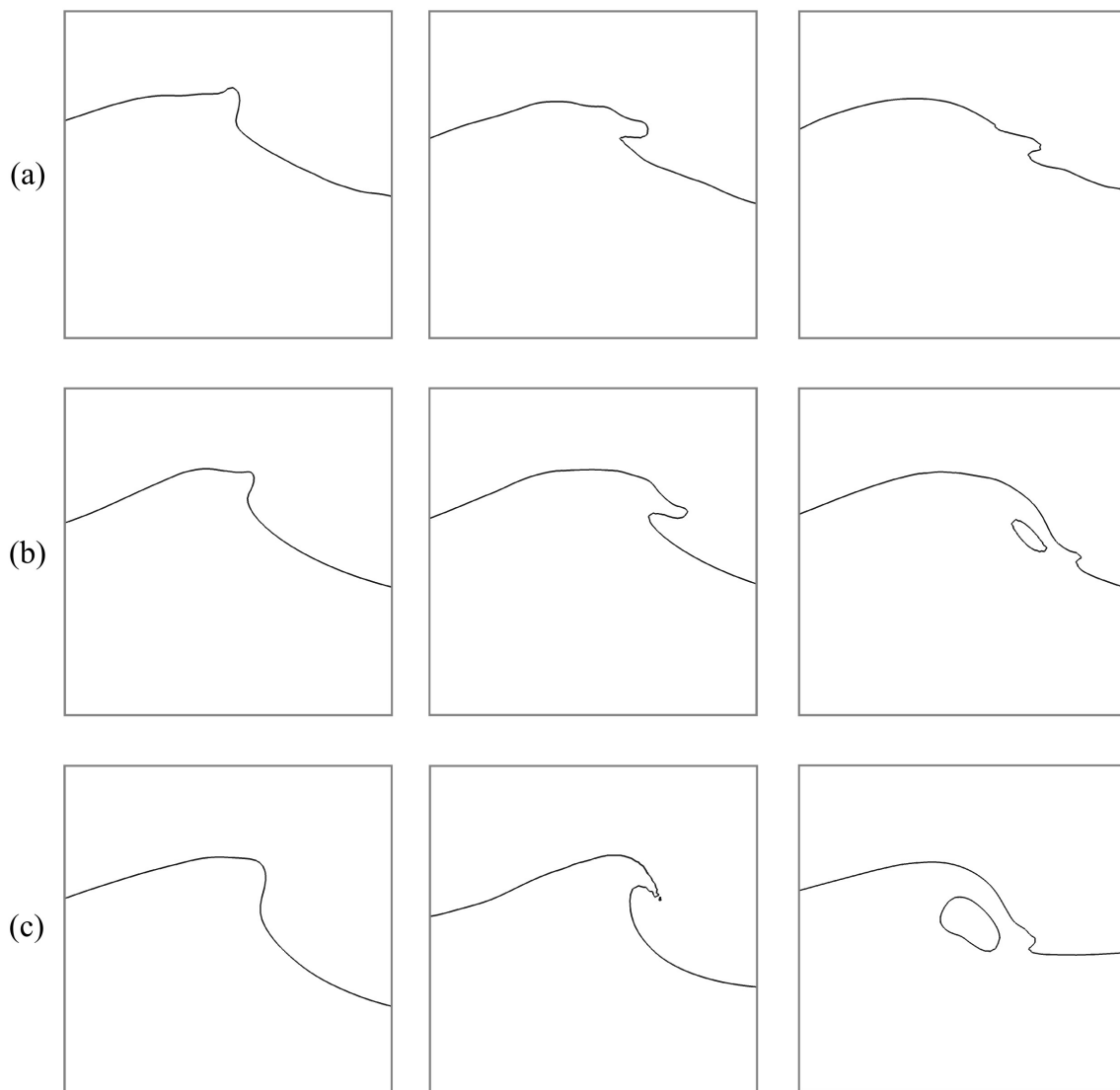
26

Figure 20: Wave profile during breaking process for different slopes and offshore wave steepness: (a) $m = 1/55$ and $H_0/L_0 = 0.06$, (b) $m = 1/15$ and $H_0/L_0 = 0.06$ and (c) $m = 1/15$ and $H_0/L_0 = 0.02$
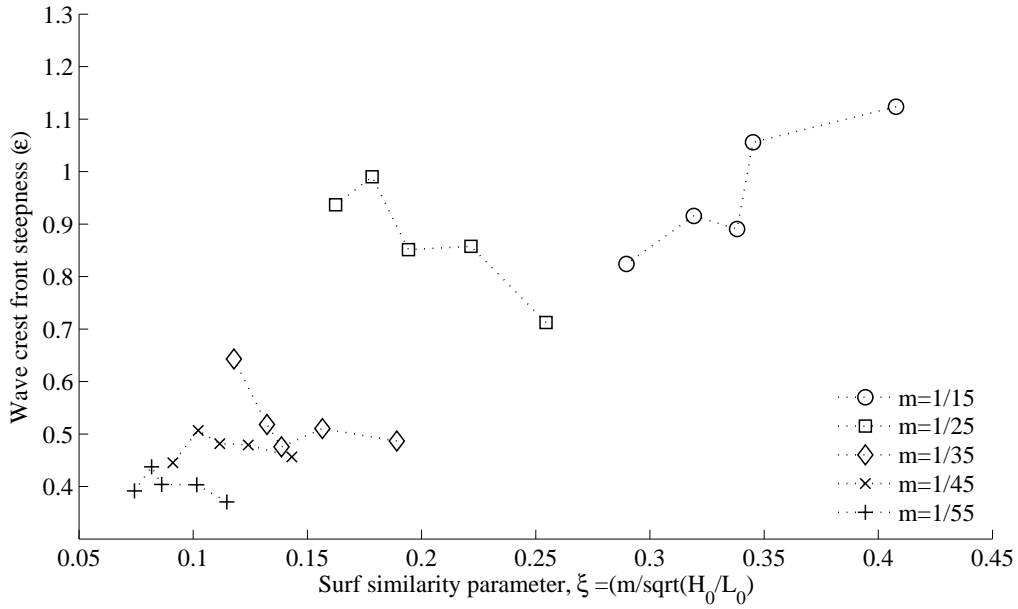
Figure 21: Computed crest front steepness (ε) as a function of surf similarity parameter (ξ) for different slopes
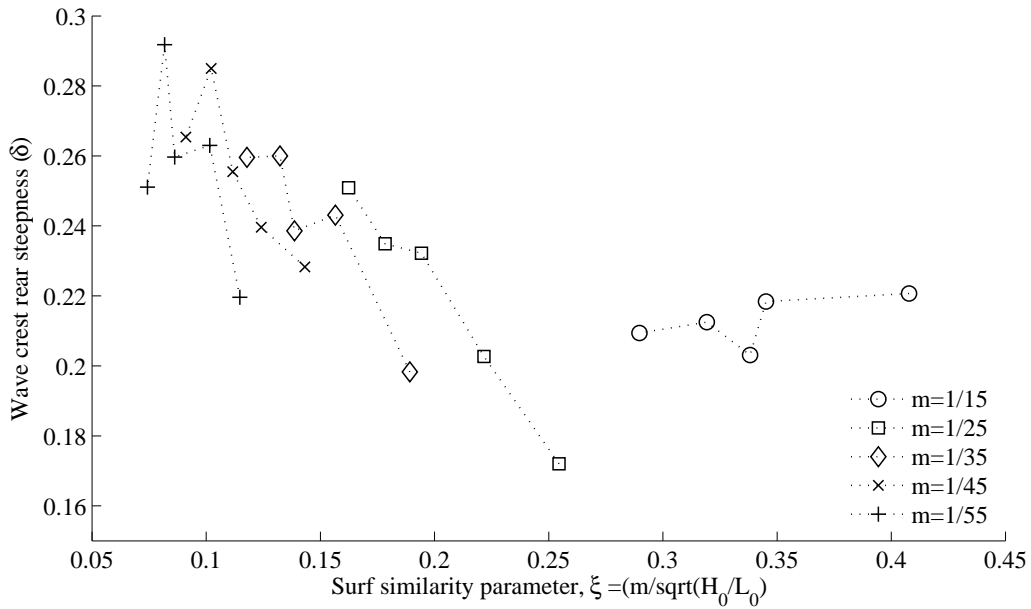

Figure 22: Computed crest rear steepness (δ) as a function of surf similarity parameter (ξ) for different slopes
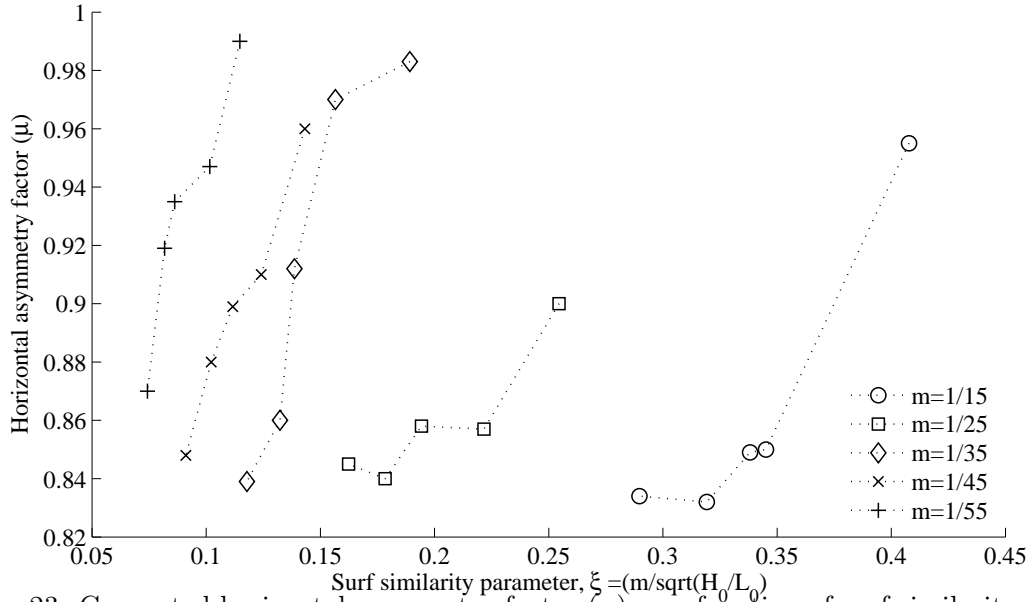
Figure 23: Computed horizontal asymmetry factor (μ) as a function of surf similarity parameter (ξ) for different slopes

is consistent with the experimental investigation of breaking waves by Lader et al. (2000). Overall, for a given H_0/L_0, ε increases and δ decreases as ξ increases. It is also noticed that the ε versus ξ dependence reduces as the seabed slope reduces.

Figs. 23 and 24 show the vertical asymmetry factor (λ) and the horizontal asymmetry factor (μ), respectively, versus the surf similarity parameter (ξ) for different slopes. It appears that μ and λ increase as ξ increases for a given slope, which is consistent with the previous results for different H_0/L_0 as shown in Fig. 19. It is also noticed that the λ versus ξ dependence decreases as the seabed slope decreases. At breaking, a wave with large H_0/L_0 propagating over a steep slope has a high and steep wave crest (i.e. large ε and μ; low δ and λ). This is clearly demonstrated in Fig. 20(b), corresponding to ξ=0.272 (case C35) and ε=0.82 (Fig. 21), δ=0.21 (Fig. 22), μ=0.83 (Fig. 23), λ=3.93 (Fig. 24). Moreover, at breaking, a wave with large H_0/L_0 propagating over a milder slope has a small portion of ejecting wave front at the crest with low crest rear steepness and a shallower wave trough as shown in Fig. 20(a), corresponding to ξ=0.074 (case C39) and ε=0.39 (Fig. 21), δ=0.25 (Fig. 22), μ=0.87 (Fig. 23) and λ=1.56 (Fig. 24). Overall, the present results of the geometrical features of spilling breakers at breaking appear to be consistent with those obtained in previous studies (Iwagaki and Sakai, 1972; Duncan, 2001; Lader, 2002).
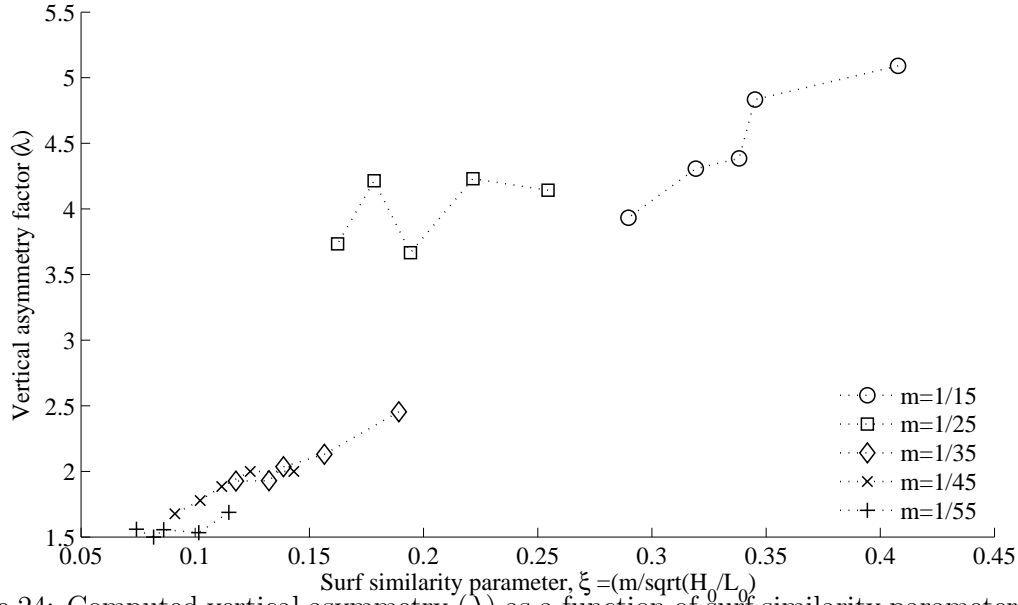
Figure 24: Computed vertical asymmetry (λ) as a function of surf similarity parameter (ξ) for different slopes

4   Conclusions

The simulation of wave shoaling and wave breaking over a sloping seabed have been studied with a two-phase flow CFD model based on the RANS equations coupled with the level set method and the $k - \omega$ turbulence model. The computed horizontal velocities and free surface elevations were compared with experimental measurements by Ting and Kirby (1996). The comparisons give good agreement between the computed results and the measured data, showing that the model can describe the wave breaking process over a slope with reasonable accuracy.

A series of numerical experiments are conducted to examine the effects of water depth, offshore wave steepness and beach slope on the characteristics and geometric properties of spilling breakers over slopes. The following conclusions can be drawn from the computational results for the different cases:

Characteristics of breaking waves

- For a given offshore wave steepness and reference water depth, the wave shoaling distance on steeper slopes is shorter, enhancing the breaking process; the waves break further offshore as the beach slope increases.

- Waves propagating over shallower reference water depth are subject to higher shoaling, break earlier at larger water depth with larger breaker height than for waves over larger reference water depth. Consequently, the breaker depth index and the breaker height index decrease with increasing reference water depth.

- For a given slope and reference water depth, waves with low offshore steepness break

30

further shoreward at shallower water depths with larger breaker height index. Therefore the breaker depth index and the breaker height index decrease with increasing offshore steepness.

- The water depth at breaking over different slopes is very sensitive to the offshore wave steepness. The shoaling rate and the partial reflections from the beach slope influence the wave breaking process. Waves with low offshore steepness over steeper slopes experience more reflections from the slope, thus the wave breaking occurs further offshore at higher water depths. On the other hand, waves with larger offshore steepness experience higher shoaling rate on milder slopes, thus the wave breaking occurs earlier than on steeper slopes.

- For wave breaking over steeper slopes, waves with low offshore steepness are greatly influenced by the partial reflection from the slope, and break faster with a higher breaker height. At the same time, waves with larger offshore steepness break shoreward at shallower water depths with lower breaker heights. The present results show that the breaker height is determined by the partial reflection on steeper slopes and by the shoaling rate on milder slopes. In fact, the breaker depth index over slopes is affected more by the water depth at breaking than by the breaker height.

Geometric properties of breaking waves

- The forward face of the wave front tends to be steeper and the rear steepness of the wave crest reduces as the reference water depth increases. Hence, the degree of asymmetry is larger and waves deform more for a larger reference water depth.

- The horizontal asymmetry and vertical asymmetry factors decrease, whereas the crest front and crest rear steepnesses increase as the offshore steepness increases. This suggests that the low offshore steepness waves are subject to more crest and trough deformation, with an overturning crest that resembles the development of plunging breakers, while waves with larger offshore steepness experience a smaller wave crest and trough deformation.

- The wave crest front steepness and the vertical asymmetry factor increase and the wave crest rear steepness and horizontal asymmetry factor decrease as the seabed slope increases. The changes in the wave asymmetry indicate that the wave front becomes vertical, the wave trough becomes deeper and the crest rear steepness of wave crest decreases as the seabed slope increases. The waves on milder slopes experience more crest deformation with an ejected wave front and a shallower trough.

Acknowledgment

References

Adeyemo, M. (1968). Effect of beach slope and shoaling on wave asymmetry. In: *Coastal Engineering Proceedings*, 145–172.

Babanin, A.V., Chalikov, D., Young, I.R. and Savelyev, I. (2010). Numerical and laboratory investigation of breaking of steep two-dimensional waves in deep water. *Journal of Fluid Mechanics*, **644**, 433. ISSN 0022-1120.

Battjes, J.A. (1974). Surf similarity. In: *Coastal Engineering Proceedings*, 1, 466–480.

Berthelsen, P.A. and Faltinsen, O.M. (2008). A local directional ghost cell approach for incompressible viscous flow problems with irregular boundaries. *Journal of Computational Physics*, **227**, 4354–4397.

Bonmarin, P. (1989). Geometric properties of deep-water breaking waves. *Journal of Fluid Mechanics*, **209**, 405–433.

Bradford, S.F. (2000). Numerical simulation of surf zone dynamics. *Journal of Waterway, Port, Coastal, and Ocean Engineering*, **126**(January/February), 1–13.

Chen, G., Kharif, C., Zaleski, S. and Li, J. (1999). Two-dimensional Navier-Stokes simulation of breaking waves. *Physics of Fluids*, **11**, 121–133.

Chorin, A. (1968). Numerical solution of the navier stokes equations. *Mathematics of Computation*, **22**, 745–762.

Christensen, E.D. (1998). *Turbulence in breaking waves - a numerical investigation*. Ph.D. thesis, Technical University of Denmark.

Christensen, E.D. (2006). Large eddy simulation of spilling and plunging breakers. *Coastal Engineering*, **53**(5-6), 463–485. ISSN 03783839.

Cokelet, E. (1977). Breaking waves. *Nature*, **267**, 769–774.

Craig, P. (1996). Velocity profiles and surface roughness under breaking waves. *Journal of Geophysical Research*, **101**, 1265. ISSN 0148-0227.

Duncan, J.H. (2001). Spilling breakers. *Annual Review of Fluid Mechanics*, **33**, 519–547.

Engsig-Karup, A.P. (2006). *Unstructured Nodal DG-FEM Solution of High-order Boussinesq-type Equations*. Ph.D. thesis, Technical University of Denmark, Lyngby.

Fenton, J.D. (1999). *The cnoidal theory of water waves*, chapter 2, 55–100. Developments in Offshore Engineering, Gulf, Houston. J. B. Herbich edition.

Galvin, C.J. (1968). Breaker type classification on three laboratory beaches. *Journal of Geophysical Research*, **73**(12), 3651–3659. ISSN 01480227.

Goda, Y. (2010). Reanalysis of regular and random breaking wave statistics. *Coastal Engineering Journal*, **52**(01), 71–106. ISSN 0578-5634.

Grilli, S.T. and Horrillo, J. (1997). Numerical generation and absorption of fully nonlinear periodic waves. *Journal of Engineering Mechanics*, **123**(10), 1060–1069.

Grilli, S.T., R. Subramanya, Svendsen, I.A. and Veeramony, J. (1995). Shoaling of solitary waves on plane beaches. *Journal of Waterway, Port, Coastal, and Ocean Engineering*, **120**(6), 609–628.

Hieu, P.D., Katsutoshi, T. and Ca, V.T. (2004). Numerical simulation of breaking waves using a two-phase flow model. *Applied Mathematical Modelling*, **28**(11), 983–1005. ISSN 0307904X.

Hwang, P.A. (1984). Profile asymmetry of shoaling waves on a mild slope. In: *Coastal Engineering Proceedings*, 1016–1027.

Ippen, A.T. and Kulin, G. (1954). The shoaling and breaking of the solitary wave. In: *Coastal Engineering Proceedings*, 27–47.

Iwagaki, Y. and Sakai, T. (1972). Shoaling of finite amplitude long waves on a beach of constant slope. In: *Coastal Engineering Proceedings*, 347–364.

Jacobsen, N.G., Fuhrman, D.R. and Fredsøe, J. (2012). A wave generation toolbox for the open-source CFD library : OpenFoam. *International Journal for Numerical Methods in Fluids*, **70**(November), 1073–1088.

Jiang, G.S. and Shu, C.W. (1996). Efficient implementation of weighted eno schemes. *Journal of Computational Physics*, **126**, 202–228.

Kjeldsen, S.P. and Myrhaug, D. (1978). Kinematics and dynamics of breaking waves. Technical report, River and Harbour Laboratory (NHL) at The Norwegian Institute of Technology.

Lader, P.F. (2002). *Geometry and Kinematics of Breaking Waves*. Ph.D. thesis, Norwegian University of Science and Technology.

Lader, P.F., Myrhaug, D. and Pettersen, B. (2000). Wave crest kinematics of deep water breaking waves. In: *Coastal Engineering Proceedings*, 355–368.

Larsen, J. and Dancy, H. (1983). Open boundaries in short wave simulations - a new approach. *Coastal Engineering*, **7**, 285–297.

Lin, P. and Liu, P.L.F. (1998). A numerical study of breaking waves in the surf zone. *Journal of Fluid Mechanics*, **359**, 239–264.

Longuet-Higgins, M.S. and Cokelet, E.D. (1976). The deformation of steep surface waves on water I- A numerical method of computation. In: *Procedings of the Royal Society of London. Series A, Mathematical and Physical Sciences*, volume 350, 1–26.

Lubin, P., Glockner, S., Kimmoun, O. and Branger, H. (2011). Numerical study of the hydrodynamics of regular waves breaking over a sloping beach. *European Journal of Mechanics - B/Fluids*, **30**(6), 552–564.

Massel, S.R. (2007). *Ocean waves breaking and marine aerosol fluxes.* Springer.

Mayer, S., Garapon, A. and Sørensen, L.S. (1998). A fractional step method for unsteady free surface flow with applications to non linear wave dynamics. *International Journal for Numerical Methods in Fluids*, **28**, 293–315.

Miller, R. and Zeigler, J. (1964). The internal velocity field in breaking waves. In: *Coastal Engineering Proceedings*, 103–122.

Osher, S. and Sethian, J.A. (1988). Fronts Propagating with Curvature-Dependent Speed: Algorithms Based on Hamilton-Jacobi Formulations. *Journal of Computational Physics*, **79**, 12–49.

Peregrine, D.H., Cokelet, E.D. and Mclver, P. (1980). The fluid mechanics of waves approaching breaking. In: *Coastal Engineering Proceedings*, 512–528.

Schultz, W.W., Huh, J. and Griffin, O.M. (2006). Potential energy in steep and breaking waves. *Journal of Fluid Mechanics*, **278**, 201.

Shu, C.W. and Osher, S. (1988). Efficient implementation of essentially non-oscillatory shock capturing schemes. *Journal of Computational Physics*, **77**, 439–471.

Southgate, H.N. (1993). Review of wave breaking in shallow water. In: *Proceedings of Advances in Underwater Technology, Ocean Science and Offshore Engineering conference*, 251–273.

Thurman, H.V. and Trujillo, A.P. (2001). *Essentials of Oceanography.* Prentice Hall.

Ting, F.C.K. and Kirby, J.T. (1996). Dynamics of surf-zone turbulence in a spilling breaker. *Coastal Engineering*, **27**, 131–160.

Tsai, C.P., Chen, H.B., Hwung, H.H. and Huang, M.J. (2005). Examination of empirical formulas for wave shoaling and breaking on steep slopes. *Ocean Engineering*, **32**(3-4), 469–483. ISSN 00298018.

van der Vorst H. (1992). BiCGStab: A fast and smoothly converging variant of Bi-CG for the solution of nonsymmetric linear systems. *SIAM Journal on scientific and Statistical Computing*, **13**, 631–644.

Vinje, T. and Brevig, P. (1981). Numerical simulation of breaking waves. *Advances in Water Resources*, **4**(2), 77–82.

Walker, J. and Headland, J. (1982). Engineering Approach to Nonlinear Wave Shoaling. In: *Coastal Engineering Proceedings*, 523–542.

Wilcox, D.C. (1994). *Turbulence Modeling for CFD.* DCW Industries Inc., La Canada, California.

Wu, C.H. (2002). Breaking criteria and energy losses for three-dimensional wave breaking. *Journal of Geophysical Research*, **107**(C10), 3177. ISSN 0148-0227.

Zhao, Q., Armfield, S. and Tanimoto, K. (2004). Numerical simulation of breaking waves by a multi-scale turbulence model. *Coastal Engineering*, **51**(1), 53–80. ISSN 03783839.